Human Molecular Genetics, 2016, Vol. 25, No. 16 3539–3554

doi: 10.1093/hmg/ddw198
Advance Access Publication Date: 13 July 2016
Original Article

ORIGINAL ARTICLE

Rescue of neural crest-derived phenotypes in a zebrafish CHARGE model by Sox10 downregulation

Zainab Asad[1,2], Aditi Pandey[1], Aswini Babu[1,2], Yuhan Sun[3], Kaivalya Shevade[1,3], Shruti Kapoor[1,2], Ikram Ullah[1], Shashi Ranjan[1], Vinod Scaria[1,2], Ruchi Bajpai[3] and Chetana Sachidanandan[1,2,*]

[1]CSIR-Institute of Genomics & Integrative Biology, South Campus, New Delhi, 110025, India, [2]Academy of Scientific and Innovative Research (AcSIR), New Delhi, 110025, India and [3]Center for Craniofacial Molecular Biology, Ostrow School of Dentistry and Department of Biochemistry and Molecular Biology, Keck School of Medicine, University of Southern California, Los Angeles, CA, USA

*To whom correspondence should be addressed at: Chetana Sachidanandan, CSIR-Institute of Genomics & Integrative Biology (CSIR-IGIB), CSIR-IGIB South Campus, Mathura Road, New Delhi 110025, India, Tel: +91-11-29879-105; Email: chetana@igib.in; chetana@igib.res.in

Abstract

CHD7 mutations are implicated in a majority of cases of the congenital disorder, CHARGE syndrome. CHARGE, an autosomal dominant syndrome, is known to affect multiple tissues including eye, heart, ear, craniofacial nerves and skeleton and genital organs. Using a morpholino-antisense-oligonucleotide-based zebrafish model for CHARGE syndrome, we uncover a complex spectrum of abnormalities in the neural crest and the crest-derived cell types. We report for the first time, defects in myelinating Schwann cells, enteric neurons and pigment cells in a CHARGE model. We also observe defects in the specification of peripheral neurons and the craniofacial skeleton as previously reported. Chd7 morphants have impaired migration of neural crest cells and deregulation of *sox10* expression from the early stages. Knocking down Sox10 in the zebrafish CHARGE model rescued the defects in Schwann cells and craniofacial cartilage. Our zebrafish CHARGE model thus reveals important regulatory roles for Chd7 at multiple points of neural crest development viz., migration, fate choice and differentiation and we suggest that *sox10* deregulation is an important driver of the neural crest-derived aspects of Chd7 dependent CHARGE syndrome.

Introduction

CHD7 is a chromodomain helicase DNA-binding domain (CHD) protein and is a member of the SWI-SNF superfamily of ATP-dependent chromatin remodelers that bind to DNA and modulate gene expression (1). CHD7 has been shown to bind to gene enhancer elements and promoters, functioning as a transcriptional co-regulator (2,3). *In vitro* assays have shown that CHD7, powered by ATP hydrolysis remodels chromatin and that disease-causing mutations identified in patients impair this function of the protein (4). CHD7 co-localizes with the histone acetyl transferase, P300 and the stem cell pluripotency factors OCT4, SOX2 and NANOG on enhancers to regulate transcription (5). The occupancy of CHD7 correlates both with activator as well as repressor functions on these enhancers (3,6), however, the functional relevance of these activities is still not completely clear.

Mutations in CHD7 cause CHARGE syndrome (OMIM ID: 214800), which is characterized by defects in multiple tissues ranging from eye, heart, craniofacial skeleton, vertebrae, genital organs, with neuronal disorders, deafness and general growth retardation (7–9). Mutations along the whole length of the

Received: May 27, 2016. **Revised:** May 27, 2016. **Accepted:** June 20, 2016

protein have been associated with CHARGE syndrome (10) suggesting that most domains in the protein are functionally important. CHARGE syndrome models have been created using morpholino based antisense oligonucleotide knockdowns of *chd7* in xenopus (11) and zebrafish (12,13), mutations and knock-outs in mouse (14,15) and drosophila (16) as well as by shRNA-based knockdown in human stem cells (11). A few of these models have identified defects in neural crest derived organs implying a conserved role for CHD7 in the neural crest.

Neural crest (NC) is a transient population of multipotent cells in the embryo that emerges from the ectoderm to migrate and populate a diverse set of tissues in the body (17). Abnormalities in many of these tissues, such as the craniofacial skeleton and peripheral nerves, are major contributors to CHARGE syndrome. In cultured human neural crest like cells (hNCLCs) CHD7 has been shown to be a part of the PBAF (polybromo-and BRG1-associated factor-containing) complex that binds to and activates enhancers of NC specific genes such as SOX9 and TWIST1 (11). CHD7 has been demonstrated to be important for maintaining multipotency of NC cells in mouse neural crest stem cells when complexed with BRG1 and other proteins (18). SOX2, a transcription factor with an important role in the epithelial to mesenchymal transition of NC cells (19), has been shown to physically interact with CHD7 to co-regulate gene expression (3). Microarray analysis of a mouse mutant for *Chd7* revealed its role in the regulation of a number of genes that are important for NC migration (20). Also, NC-specific conditional deletion of *Chd7* in mouse causes deformities in the craniofacial skeleton (21). However, the role of Chd7 in the various stages of neural crest development and differentiation has not yet been explored.

Here we investigate the effects of *chd7* knockdown on the development and differentiation of zebrafish neural crest. We show that chd7 deficiency affects early NC gene expression as well as NC migration. We demonstrate that Chd7 is critical for fate determination of NC derivatives and that its deficiency adversely affects crest-derived precursor as well as differentiated populations of craniofacial cartilage, cranial ganglia and enteric neurons. We find that Chd7 is crucial for the differentiation of pigmented cells and myelinated Schwann cells, which has not been reported previously. In the *chd7* morphants we also observed a deregulation of the transcription factor *sox10*, known for its role in neural crest. By reducing the levels of Sox10, we could rescue a number of different crest-derived phenotypes indicating the importance of *sox10* deregulation in the pathophysiology of CHARGE.

Results

chd7 RNA is inherited from parents and ubiquitously expressed in early zebrafish embryos

CHD proteins play important roles in development, stem cell function, adult physiology and diseases (1,22). To determine the expression of these genes in zebrafish, we analysed existing RNA sequencing data available in the public domain for different developmental stages and tissues of zebrafish [SRP009426 (23), SRP008845 (24), ERP000016 (Zebrafish transcriptome sequencing project, PRJEB1986), PRJNA207719 (25) and SRP017135 (26)] . We found expression data for 10 members of the chd family. *Chd1-like, chd2, chd3, chd6 and chd9* had very low expression at most stages of zebrafish development, while *chd1, chd8, chd4a* and *chd4b* showed high expression in some tissues and stages (Fig. 1B). The most abundant chd mRNA in zebrafish was *chd7* (Fig. 1B).

Chd7 expression was maximum in the early stages of development starting from 2 to 4 cells (Fig. 1A). In zebrafish embryos, the zygotic transcription starts between 1K cell stage and dome stage (3–4 hours post fertilization (hpf)) (27), thus mRNA present in 2–4 cell and 1K cell stages are indicative of parental contribution. The only adult tissue with comparable expression to the early embryonic stages was the ovary (Fig. 1A). *Chd7* could be amplified from both adult zebrafish ovary and testis cDNA (Fig. 1C), suggesting that the contribution of the *chd7* transcript to the zygote could be from both parents.

To confirm observations made from RNA sequencing analysis and to understand the spatial distribution of the *chd7* RNA, we performed RNA *in situ* hybridization at various embryonic stages (Fig. 1D–J). Reinforcing the RNA sequencing data, *chd7* was highly expressed from 2-cell stage onwards (Fig. 1D). Ubiquitous expression was observed at 2-cell, 8-cell, sphere and 10-somite stage (Fig. 1D–G). CHD7 is known as a positive regulator of ribosomal RNA biogenesis in stem cells (6) and might be essential in the first few hours when the translation of maternal RNA is essential for the rapid progression of embryonic development. By 24hpf, the expression becomes more restricted to the head, specifically in the eye and the mid-and hindbrain (Fig. 1H and I), as has also been shown previously (12,28). At 4 days post fertilization (dpf), *chd7* expression was visible in the pineal complex, midbrain-hindbrain boundary, eye, jaw region and the gut tube (Fig. 1J) which supports previous studies showing the important roles for Chd7 in neurogenesis in the embryo as well as the adult (29,30).

Knockdown of *CHD7* in Zebrafish

To address the role of Chd7 in zebrafish development, we designed a splice blocking antisense morpholino oligonucleotide (MO) against the exon8-intron8 boundary (MO1) (Supplementary Material, Fig. S1B). The MO1 would be predicted to cause retention of intron8 in the processed transcript (Supplementary Material, Fig. S1C). PCR analysis of the cDNA from embryos injected with 2.4ng of *chd7* MO1 confirmed the presence of a defective splice product; (Supplementary Material, Fig. S1D). We amplified the aberrant splice-product from cDNA of both control MO and *chd7* MO1 injected embryos using primers in the exon6 and intron8 (Supplementary Material, Fig. S1B and S1C). The control embryos had no detectable expression of the aberrant product while the chd7 morphant embryos had a robust expression (Supplementary Material, Fig. S1D). The product size matched retention of only intron8 and not intron6 or intron7 also confirming that the aberrant product was the result of splicing defects, not genomic DNA contamination in the cDNA. We further amplified the exon8-intron8 boundary by PCR from the morphant cDNA and sequenced this amplicon to confirm the retention of intron (Supplementary Material, Fig. S1E). The insertion of the intron8 would be predicted to cause a frame shift mutation in the *chd7* transcript resulting in a 943 amino acid long protein, instead of the 3140 amino acid long full-length Chd7 protein (Supplementary Material, Fig. S1A). The truncated form of Chd7 is predicted to contain only the chromodomain-1 and to lack all other known domains of the Chd7 protein. Similar was the case when we injected a previously published *chd7* morpholino (MO2) (13) that is predicted to result in a 1447 aa Chd7 protein product (Supplementary Material, Fig. S1A).

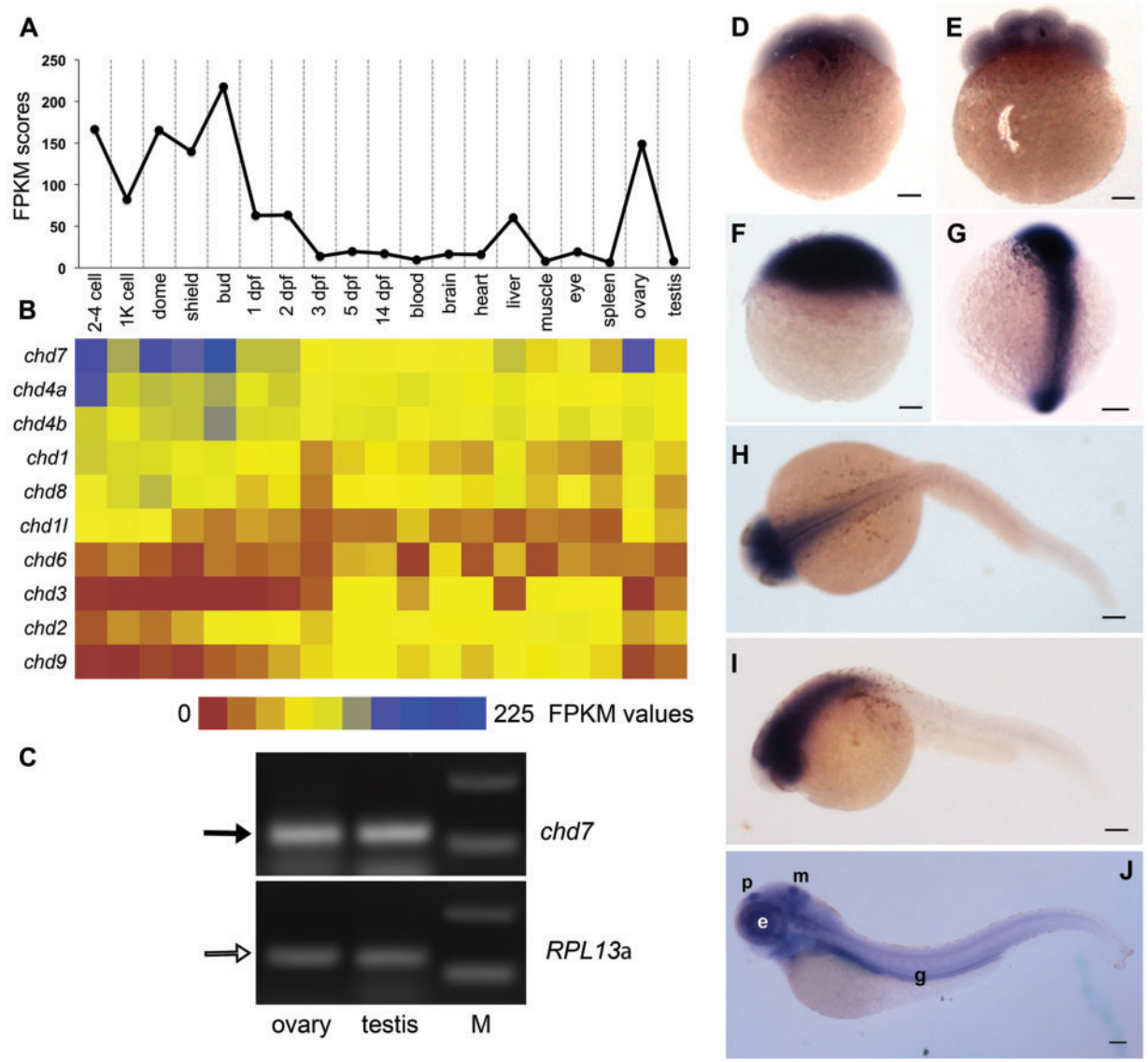

Figure 1. Parental contribution and ubiquitous expression of *chd7* in the early stages. **(A)** FPKM scores for *chd7* plotted at different stages and tissues. Highest expression is seen in 2–4 cell, dome stage and bud stage. In adult tissues, ovary had the highest expression. **(B)** Heatmap depicting FPKM values from RNA sequencing analysis (from data available in the public domain) of 10 chd transcripts across different zebrafish developmental stages and tissues. *chd7* is the most abundant mRNA among the Chd group of proteins. **(C)** Agarose gel electrophoresis showing amplification of *chd7* transcript (black arrow) from adult ovary and testes, suggesting maternal and paternal contribution of *chd7* to zygote. *RPL13α* (white arrow) is used to normalize the RNA levels. **(D–G)** chd7 is ubiquitously expressed in early stages. RNA *in situ* hybridization of chd7 in zebrafish embryos at 2-cell (D), 8-cell (E), dome (F) and 10-somite stage (G) shows ubiquitous expression. The animal pole is to the top (D–F). Dorsal view, anterior to the top (G). **(H–I)** At 24hpf, expression of chd7 is restricted to the head. **(J)** 4dpf larva expresses chd7 more in the eye, pineal gland-p, midbrain-hindbrain boundary-m and gut tube-g. Anterior is to the left. (H) dorsal view, (I,J) lateral view. The scale bar marks 100μm.

Injection of 2.4ng *chd7* MO1 caused developmental defects without causing lethality and all following experiments in this study were performed at this concentration of the MO1, unless otherwise mentioned. From hereon, we refer to *chd7* MO1 as *chd7* MO (and where MO2 has been used, it is explicitly stated). All the control embryos were injected with equal amount of a control MO with random scrambled sequence from Gene Tools®.

Injection of *chd7* MO caused multiple morphological defects including small head and eyes, missing or reduced jaw and pericardial edema (Fig. 7B). In order to determine if the phenotypes are due to downregulation of Chd7, we co-injected 1.5ng of full-length human *CHD7* RNA (11) with 1.2ng of *chd7* MO. The expression of the human *CHD7* RNA was determined by PCR of 24hpf injected embryos (Supplementary Material, Fig. S1F). Craniofacial defects have been noted in *chd7* morphant zebrafish previously (13). Four-day old *Tg(sox10:eGFP)* larvae had GFP expression in the craniofacial cartilage stacks (Supplementary Material, Fig. S1G). In larvae injected with *chd7* MO severe defects in the craniofacial cartilage was evident. Co-injection of wildtype human *CHD7* RNA with the *chd7* MO partially rescued the craniofacial defects in the morphant larvae (Supplementary Material, Fig. S1G). No rescue was observed in larvae co-injected with *chd7* MO and dsRed RNA. Thus, human CHD7 is able to replace the loss of zebrafish Chd7 suggesting a high degree of functional conservation between species.

These observations also reinforce that the phenotypes observed in the *chd7* MO are caused specifically due to reduction of Chd7 activity.

Chd7 Regulates Neural Crest Gene Expression and Migration

Many NC-derived cell types such as craniofacial cartilage and cranial motor and sensory neurons are affected in the CHARGE syndrome and Chd7 has been implicated in the development of NC derived cell types (11,18,21). However, no study has examined the role of Chd7 in the NC cells in detail. We set out to systematically dissect the effect of *chd7* knockdown on NC in the zebrafish embryos, as a model for vertebrate development. We began by analysing 3-somite stage (ss) embryos; around the stage when NC cells are specified. Expression of one of the earliest NC specification markers snai2, is reduced in the *chd7* morphants (Fig. 2A and B) while levels of *tfap2a* and *foxd3*, both early markers of NC cells, appear largely unperturbed in the morphants compared to the controls (Fig. 2C and 2F). *sox9a*, an SRY box gene that is crucial for NC specification and migration, is severely downregulated (Fig. 2G and H). Thus, the neural crest appears to be specified but not patterned correctly in the *chd7* morphants, perhaps eventually influencing the downstream steps in NC development.

Since NC cells delaminate from the neural tube, we analysed the expression of *sox2*, a neural tube marker. Expression of *sox2*, is significantly downregulated in *chd7* MO injected embryos (Fig. 2I and J). Human fetuses with *CHD7* mutation have been known to have neural tube defects (31). It is possible that some of the effects on NC could be secondary to the defect in neural tube patterning.

We followed the expression of *foxd3* into the 18-somite stage embryos. *foxd3* is expressed in pre-migratory NC cells and in the

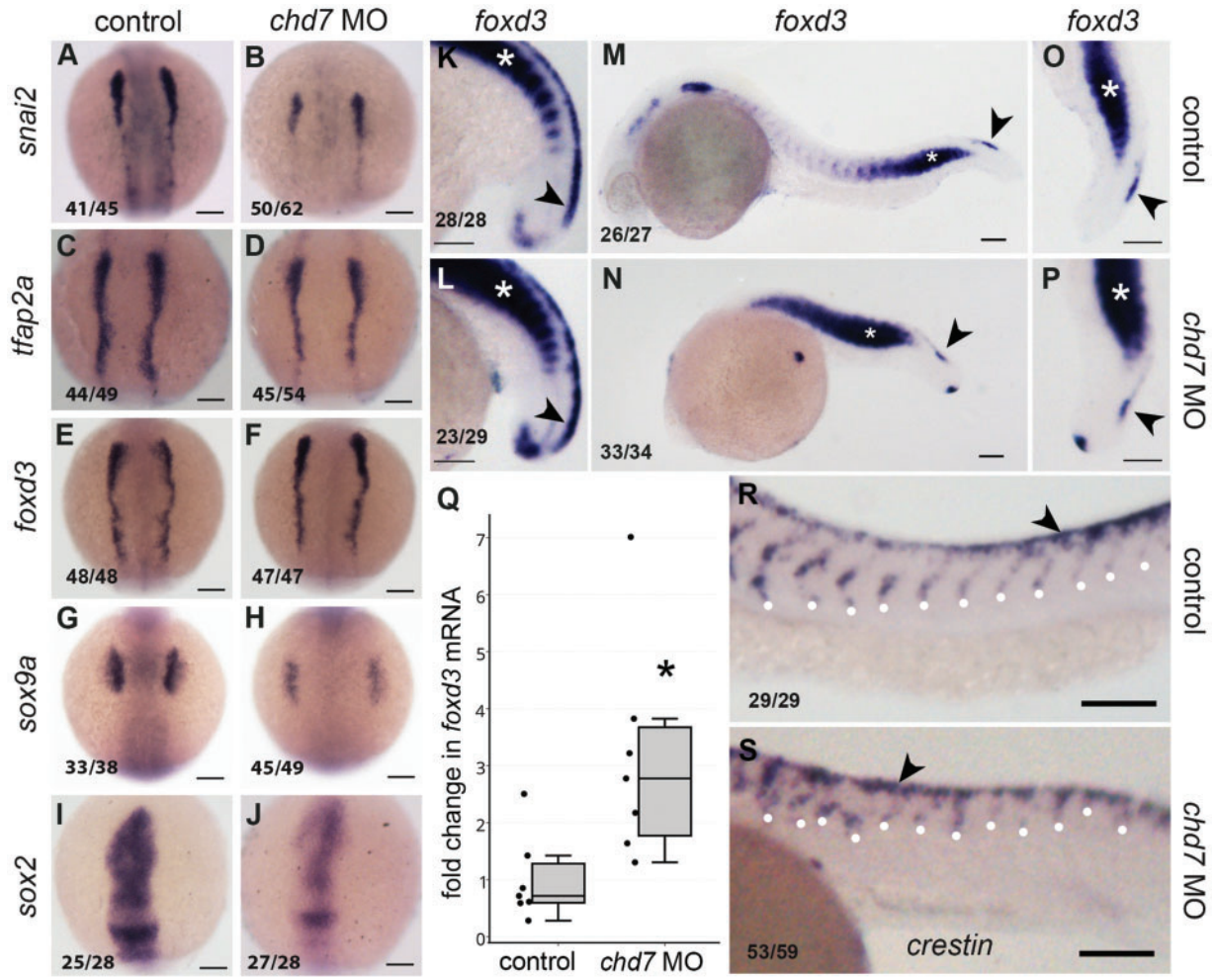

Figure 2. *chd7* knockdown causes differential effects on neural crest markers and impairs neural crest migration. RNA *in situ* hybridization of neural crest markers at 3 somite **(A–J)**, 18 somite **(K–L)** and 24hpf **(M–P** and **R–S)** stages; control (A, C, E, G, I, K, M, O, R) and *chd7* morphant (B, D, F, H, J, L, N, P, S) embryos. (A,B) *snai2*, the earliest marker of neural crest specification was downregulated in *chd7* morphant, while early neural crest markers *tfap2a* (C,D) and *foxd3* (E,F) appeared unaffected. (G, H) sox9a was downregulated in the *chd7* morphants. (I, J) *sox2*, a marker of neural tube, was downregulated in the *chd7* morphants. Dorsal views, with anterior to the top (A–J). (K,L) At 18hpf, the somitic (white asterisk) and crest expression (black arrowhead) of *foxd3*, was upregulated in morphants. (M–P) However at 24hpf, foxd3 was predominantly upregulated in somites (white asterisks) while the expression in caudal neural crest was unchanged (black arrowheads) in *chd7* morphants. (O,P) magnified views of trunk region of m, n. (Q) Quantitative real time PCR analysis of *foxd3* mRNA shows upregulation in 24hpf *chd7* morphant embryos (3.13 fold, $P < 0.05$). (R,S) *crestin*-marked neural crest cells migrate robustly in controls but are stalled near the dorsal crest in chd7 morphants (white dots mark the point of migration). Lateral views with anterior to the left, dorsal to the top (K–P, R–S). All scale bars are 100μm. The numbers in the bottom left corner indicate the actual number of embryos of the total represented by the image.

somites in the 18-somite stage embryos (Fig. 2K and L) and there is an upregulation of both domains of expression in the *chd7* morphants. At 24hpf, the NC-specific expression of *foxd3* remains only in the caudal-most region and this appeared unperturbed in the *chd7* morphants (Fig. 2M and P). *Foxd3* is also expressed robustly in the somites and this expression was significantly upregulated in the morphants (Fig. 2M and P). *Foxd3* has been implicated in regulation of *myf5* (32), the myogenesis factor expressed in the somites as they differentiate to myoblasts. The *foxd3* deregulation may suggest possible skeletal muscle-related complications in CHARGE. We performed quantitative RT-PCR of 24hpf embryos and found an average 3.13 fold upregulation of *foxd3* mRNA (Fig. 2Q). A recent study compared the RNA profiles of wildtype and whirlgig ($chd7^{wg/wg}$) mouse embryos during NC migration (9.5dpc) using microarray and they found a 2.5 fold upregulation of *foxd3* in the $chd7^{wg/wg}$ mouse embryos (20). Our whole organism analysis suggests that the overall upregulation evident in the *chd7* mutant/morphant background may be primarily attributed to the somitic expression.

By 24hpf NC cells are rapidly migrating in a rostral-to-caudal chronology. Thus, the cranial and vagal cells have completed their migration while the trunk NC may be seen in different stages of the migration as visualized by crestin, a NC marker (33). Trunk migration was severely impaired in the *chd7* morphants and cells appear to be still residing in the dorsal position when compared to the control embryos (Fig. 2R and S). This data supports previous studies on human NC like cells (hNCLC) and Xenopus embryos, which demonstrated that NC cell migration is impaired upon *CHD7* knockdown (11).

Chd7 Deficiency Causes Deregulation of *sox10* Expression

A critical regulator of neural crest cell specification, migration and fate choice, is Sox10. We analysed the expression of *sox10* in *chd7* morphants from 3ss, when the NC is first evident, to 4dpf, when many NC derived cells are undergoing differentiation, in zebrafish embryo. We mapped *sox10* expression in the 3ss (11hpf), 6ss (12hpf), 10ss (14hpf), 14ss (16hpf), 18ss (18hpf) and 22ss (20hpf) embryos. The embryos were staged by counting somites (till 22ss) to confirm the developmental stage. The 3ss control embryos expressed *sox10* in the neural plate border cells while in *chd7* morphant embryos this expression was not very apparent (Fig. 3A and B). By 6ss the control NC cells were migrating medially (also described in (34), however the NC in the *chd7* morphants were still farther apart and there was no evidence of medial migration (Fig. 3C and D). As the vagal and cranial NC condense at 10ss, the medial migration was no longer evident in the control, but appeared to continue in the *chd7* morphants (Fig. 3E and F). In lateral views of the embryos the NC, marked by *sox10* expression, stretches caudally to more than half the length of the embryo, while in the *chd7* morphants the crest was seen only in the anterior trunk region (Fig. 3G and H). In the 14ss (Supplementary Material, Fig. S2A and S2B) and 18ss embryos (Fig. 3I and L), *sox10* marks the ventrally streaming NC cells and these streams were absent or severely reduced in the chd7 morphants; this effect was also evident in 20hpf embryos (Supplementary Material, Fig. S2C and S2D). In summary, we observed that the *sox10* expression pattern in the *chd7* morphants was reminiscent of expression in the control embryos, but a few hours younger, indicating a delay specifically in the NC development.

At 24hpf, as the NC completes their migration, *sox10* is downregulated in these cells. In the control embryos, *sox10* expression decreased rapidly and was found only in the occasional dispersed cells and in the yet-to-migrate caudal crest (Supplementary Material, Fig. S2I). We observed that at 24hpf, the *chd7* morphant embryos have impaired NC migration and retain a robust expression of *sox10* in the dorsal crest region (Supplementary Material, Fig. S2J). This effect on *sox10* was confirmed independently in *chd7* MO2 injected embryos (Supplementary Material, Fig. S2O and S2P). By quantitative RT-PCR, we observed an average 2.7 fold increase in *sox10* gene expression in the *chd7* morphant embryos (Fig. 3T). Schulz *et al.* as described in the previous section, in their microarray analysis on wildtype and whirlgig ($chd7^{wg/wg}$) 9.5dpc mouse embryos also reported a 2.2 fold upregulation of *sox10* RNA in the $chd7^{wg/wg}$ embryos (20).

To determine if the increase in *sox10* RNA impacts the protein expression, we performed immunostaining with an anti-Sox10 antibody in 24hpf embryos. We found that the *chd7* morphant embryos had more cells expressing Sox10 protein compared to the controls (Fig. 3M and N). We used the *Tg(–4.9sox10:egfp)*^{ba2} line to visualize the migrating NC in live embryos at 24hpf and observed a similar increase in the number of GFP positive cells in the morphants when compared to controls (Fig. 3O and P). We quantified this effect using flow cytometry and found a 1.7 to 3.5 fold increase in the number of GFP positive cells in the *chd7* morphants (Fig. 3S).

The increase in *sox10* expressing cells at 24hpf may be attributed to the delay in migration and the concomitant delay in downregulation of Sox10 in migrating NC cells. However, we observed that the elevation in Sox10 expression was not confined to the 24hpf morphant embryos. We observed ectopic and elevated expression of *sox10* in 28hpf *sox10:eGFP* morphant embryos (Supplementary Material, Fig. S2K–S2N) and in 36hpf *chd7* MO embryos by RNA *in situ* hybridization (Supplementary Material, Fig. S2M and S2N). Examination of 4dpf *sox10:eGFP* larvae by microscopy showed that the control larvae have a clear pattern of fluorescence in the spinal cord but little elsewhere (Fig. 3Q). The *chd7* morphant larvae did not have a very strong fluorescence in the spinal cord, however there was ectopic fluorescence in the trunk region (Fig. 3R). Thus, we conclude that *chd7* morphant animals have an overall deregulation of *sox10* expression from the early NC stages to later.

chd7 Knockdown Affects Migration of Pigment Precursors and Inhibits Differentiation of Pigment Lineages

Sox10 is a crucial transcription factor for pigment development in vertebrates (35). Zebrafish has two different kinds of pigment cells melanophores and iridophores that are derived from same precursor pool of NC cells and regulated by Sox10 (36). Since *sox10* is deregulated in the *chd7* morphant fish, we analysed the status of these pigments in 5dpf zebrafish larvae. Iridophores produce the iridescent pigment in the eyes, top of the head, body and in discrete spots on the trunk in 5dpf control larvae (Fig. 4A). We found an absence of the iridophores (or rather the iridescent pigment) in the whole body of *chd7* morphant larvae (Fig. 4B) (previously reported in the eye (12)). Melanophores that contain the black pigment melanin are evident by 30hpf in zebrafish embryos (37) and we observed that 2dpf and 5dpf *chd7* morphant animals had decreased pigmentation. At 5dpf, the melanophore shape also appeared to be abnormal in the

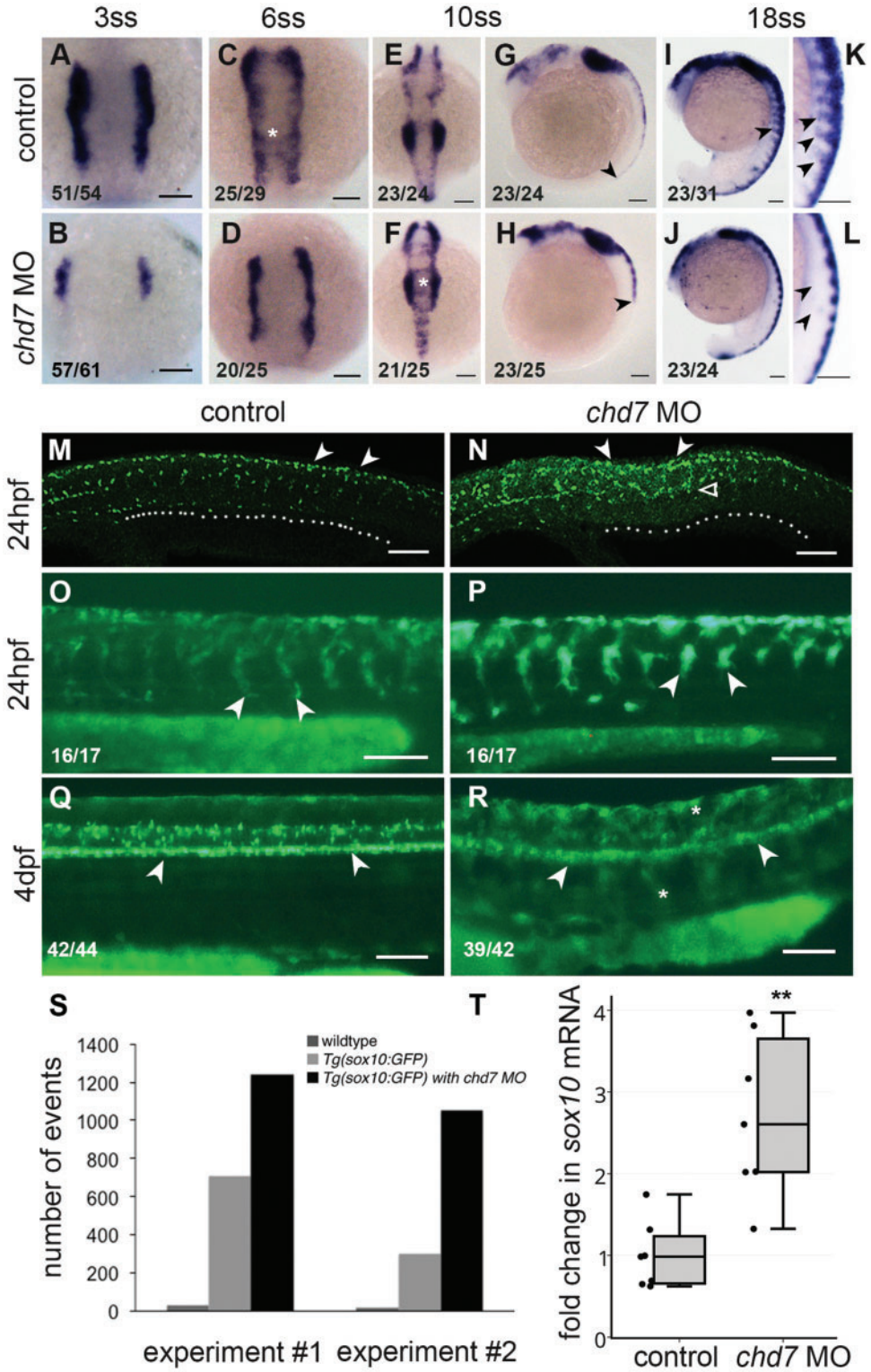

Figure 3. *Chd7* knockdown causes deregulation of *Sox10* expression in the neural crest. **(A–L)** RNA *in situ* hybridization of *sox10* at different stages; control (A, C, E, G, I, K) and *chd7* morphant (B, D, F, H, J, L). (A, B) At 3 somite stage (ss), *Sox10*, expressed in neural plate border cells is less in *chd7* morphants. (C,D) At 6ss, the NC cells begin migration medially (asterisk) in control but not in *chd7* morphants. (E–H) At 10ss, the medial migration concluded, cells condense in the vagal and cranial regions, while the *chd7* morphants continue medial migration (asterisk) Dorsal views, with anterior to the top (A–F). (G, H) Lateral views of 10ss embryos shows that the NC stretches caudally to more than half the length of the control embryo, while in the *chd7* morphants the crest was seen only in the anterior trunk region (black arrowheads). (I–L) At 18ss, *Sox10* marks the ventrally migrating streaks of NC cells, which were absent or severely reduced in the *chd7* morphants. (K, L) are magnified images of (I, J). Lateral views, with anterior to top (G–L). **(M,N)**. At 24hpf, Sox10 antibody stained cells which have migrated to ventral region of embryo in control (white dots) while in chd7 morphant Sox10 positive cells have travelled only halfway (white open arrowhead) and are accumulated at the dorsal crest (white arrowheads). **(O–P)** At 24hpf, Tg(*sox10*:eGFP) marks NC cells that have migrated to the ventral-most region while *chd7* morphant showed retention of GFP expression and abnormal migration of NC

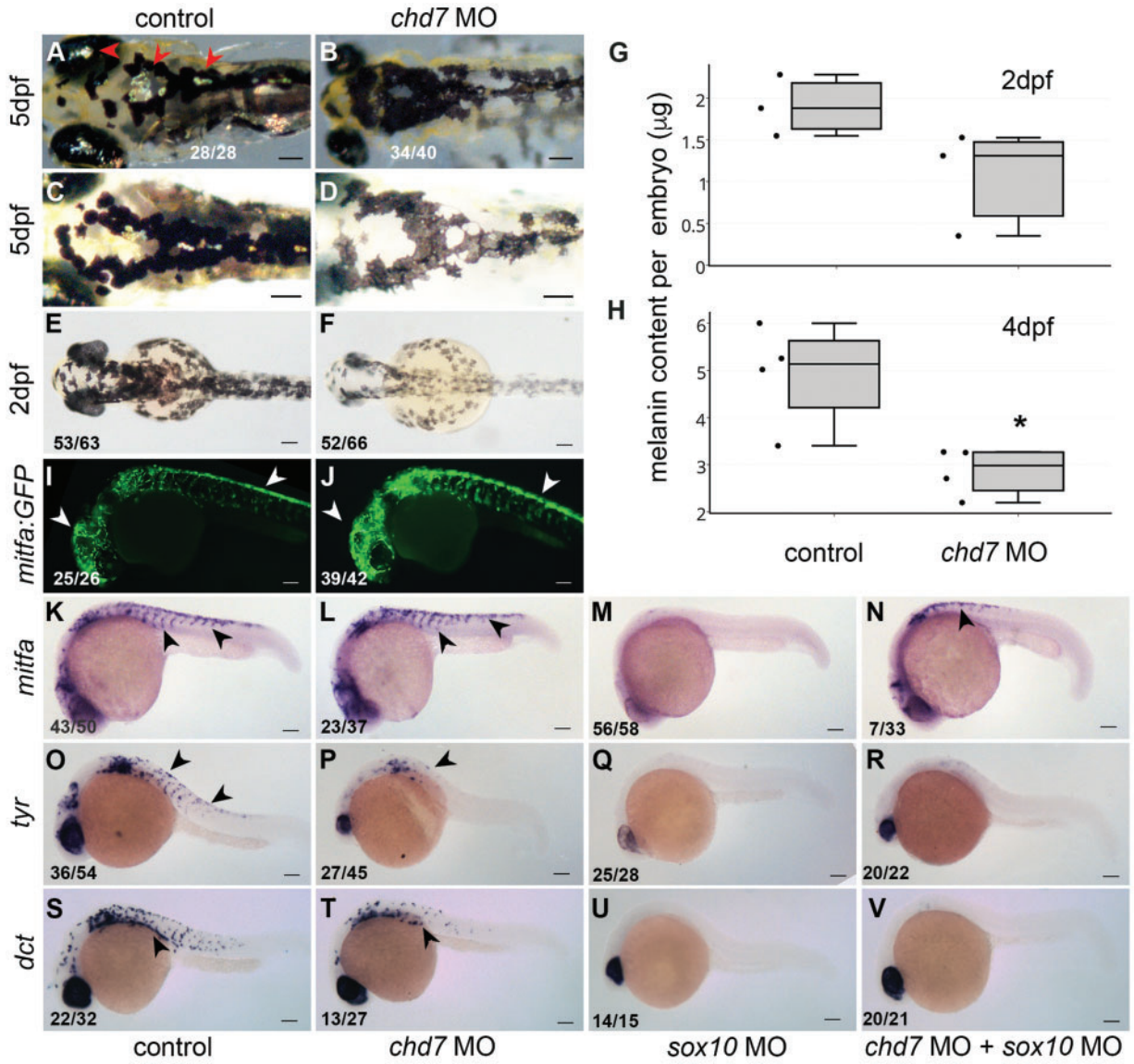

Figure 4. *chd7* MO affects migration of pigment precursors and inhibits differentiation of pigment lineages. **(A–B)** At 5dpf, embryos had iridescent iridophores present in eye and body (red arrowheads, a) while iridophores were absent in *chd7* morphants. **(C–D)** At 5dpf, embryos had condensed dark melanophores, while *chd7* morphants had spread out dentritic shaped melanophores with overall less melanin. **(E–F)** 2dpf control embryos are darker than the *chd7* morphants. **(G–H)** Relative melanin content was decreased mildly in 2dpf (1.8 fold, ns) and significantly in 4dpf (1.7 fold, $P < 0.05$) *chd7* morpholino injected larvae. **(I, J)** *Tg(mitfa-GFP)* marks the melanoblasts at 24hpf, and these are distributed in the head and dorsal crest region (white arrowheads, I), while, *chd7* morphants had expanded population of *mitfa:GFP* positive cells in both the regions (white arrowheads, J). **(K,L)** mitfa *in situ* hybridization at 24hpf marks the melanoblasts in crest and head region, however *chd7* morphants had elevated *mitfa* expression mostly in the dorsal crest. **(M,N)** *sox10* MO injected embryos had no *mitf-a* expression apparent, while embryos coinjected with *sox10* MO and *chd7* MO had less *mitf-a* expression than *chd7* MO alone. **(O–R)** RNA *in situ* hybridization of *tyrosinase* marks differentiated melanophores in 24hpf embryos. *chd7* morphants had severe downregulation of tyrosinase. *Sox10* morphants also had complete absence of *tyr*, which was not recovered in embryos coinjected with *chd7* and *sox10* MO. **(S–V)** RNA *in situ* hybridization of *dct* also marks differentiated melanophores in 24hpf embryos. *chd7* morphants had severe downregulation of *dct* as did *sox10* morphants. The *dct* expression was not recovered in embryos coinjected with *chd7* and *sox10* MO. All images have anterior to the left; dorsal views (A–F) and lateral views (I–V). All scale bars are 100µm. The numbers in the bottom left corner indicate the actual number of embryos of the total represented by the image.

cells that have stuck midway (white arrowheads). **(Q–R)** At 4dpf, *Tg(sox10:eGFP)* shows *sox10* expression in spinal cord (white arrowheads), however in *chd7* morphant embryo spinal cord expression was not so evident but ectopic GFP positive cells appeared in the trunk region (white asterisks). Lateral views with anterior to left (M–R). **(S)** Flow cytometry analysis of *sox10*:eGFP positive cells showed a 1.7 fold to 3.5 fold expansion of GFP positive cell population in the *chd7* morphants **(T)** Quantitative real time PCR analysis of *sox10* mRNA showed upregulation in 24hpf *chd7* morphant embryos (2.7 fold, $P < 0.01$). All scale bars are 100µm. The numbers in the bottom left corner indicate the actual number of embryos of the total represented by the image.

morphants (Fig. 4C and D). We quantified the melanin content per embryo in 2dpf and 4dpf animals and found a significant decrease in the *chd7* morphants compared to controls (Fig. 4G and H).

The differentiation of melanophores is initiated by the transcription factor *mitf-a* which is expressed in the precursors of melanophores as they migrate laterally from the crest (38). The *mitf-a* positive NC cells are marked by GFP in the *Tg(mitf:GFP)* transgenic line. At 24hpf, the *chd7* morphant embryos have elevated levels of GFP (Fig. 4I and J) compared to controls. RNA *in situ* hybridization of *mitf-a* showed delayed migration and dorsal accumulation similar to that seen in *sox10* (Fig. 4K and L). Melanophores express two enzymes that are important for melanin formation, *tyrosinase (tyr)* and *dopachrome tautomerase (dct)* (39). The expression of these genes is evident in distinct scattered cells throughout the embryo at 24hpf (Fig. 4O and S); this expression is severely downregulated in the *chd7* morphants (Fig. 4P and T).

It is important to note that CHARGE patients have not been reported to have any pigmentation defects. Melanophore development is known to be very plastic and alternate routes of melanogenesis may become active even when the primary wave of melanogenesis is compromised (40). It is possible that the requirement for Chd7 by melanophores is species specific and is not necessary in the human melanocytes.

Knockdown of *sox10* in Zebrafish Embryos

Since an upregulation of *sox10* was noticed in the neural crest of the *chd7* morphant (Fig. 3M and P) embryos and *sox10* is a known regulator of mitf-a (41), we sought to downregulate Sox10 levels using a MO. We used two *sox10* MOs in this study: MO1, a translation blocking MO (42) and MO2, a splice blocking MO (designed for this study, details in Supplementary material Table S1 and Supplementary Material, Fig. S3B). The *sox10* MO1 (henceforth referred to as *sox10* MO) is predicted to block the translation and immunostaining of *sox10* MO injected embryos with anti-Sox10 antibody showed a dramatic reduction in the protein levels in 24hpf embryos (Supplementary Material, Fig. S3C). *sox10* MO2 injection would be predicted to interfere with the splicing of exon2 and exon3 causing either retention of intron2 or loss of exon3 (Supplementary Material, Fig. S3D). We performed a PCR with primers on exon2 and exon4 and found that there was no detectable product in the morphant, as predicted if the 2kb long intron is retained in the morphant (Supplementary Material, Fig. S3E). We performed another PCR with primers in exon2 and exon3 and also found significant downregulation of the 382bp PCR product (Supplementary Material, Fig. S3D,S3E,S3F) confirming the aberrant splicing in the *sox10* MO2.

Sox10 Downregulation Does Not Affect The Pigment Defect in *chd7* Morphant Zebrafish

We examined the embryos after injection of the *Sox10* MO for the pigmented melanocytes and pigment regulatory genes. As would be expected, *Sox10* MO injected embryos exhibited a reduced pigment phenotype [as previously shown in (43); Supplementary Material, Fig. S4G]. *Sox10* MO caused a complete loss of tyr, dct as well as mitf-a (Fig. 4M,Q,U). *sox10* MO2 elicited a similar but weaker effect (Supplementary Material, Fig. S4N–S4S). Coinjection of *chd7 MO* and *sox10* MO caused a downregulation of mitfa RNA, compared to the *chd7* MO alone suggesting a role for Sox10 in the elevated levels of *mitf-a* (Supplementary Material, Fig. S4I). However, the double morphant embryos continued to have severe effects on the migration of *mitf-a* positive NC (Fig. 4N). The double morphants did not show any recovery of the expression of the melanophore differentiation factors tyr or dct (Fig. 4R and V, Supplementary Material, Fig. S4J and S4K). This indicated that chd7 may also play an independent role in the induction of differentiation genes in the melanophore precursors. Recent studies have shown that the MITF regulatory complex, which includes BRG1, that is responsible for induction of melanocytic genes, contains multiple chromatin modifying proteins, including CHD7 (44). Thus, although Sox10 along with Mitfa is known to activate the differentiation genes *dct* and *tyr* (45) *chd7* may also be essential for the induction of differentiation in the pigment lineage, independent of the deregulation of Sox10.

Loss of CHD7 Causes Reduction of Peripheral Neuronal Lineages

Neuronal defects are a hallmark of CHARGE syndrome. CHARGE patients have multiple defects such as defects in facial muscles, xvestibular functions, hearing, olfaction and swallowing difficulties (9). The peripheral nervous system consists of neurons and glia derived from the neural crest. We probed the different peripheral neuronal lineages in our model for CHARGE syndrome. Cranial neurons include both sensory and motor neurons that control functions in the head and face. We detected differentiated cranial neurons in 72hpf embryos using *islet-2a (isl2a)*(46) as a marker and discovered that knockdown of *chd7* leads to a dramatic reduction of these neurons (Fig. 5A and B). This is also substantiated by a previous study in zebrafish (12). Since the cranial neurons are reduced in *chd7* morphants, we probed the status of the cranial neuron precursors in the epibranchial ganglia marked by neuroD (47) at 36 hpf; this expression was severely reduced in the *chd7* morphant embryos (Fig. 5C and D) suggesting that the defects begin in the precursor populations. The *chd7* MO2 had similar effects on *neuroD* and *isl2a* expression (Supplementary Material Fig. S5J and S5K and S5N–S5O).

Enteric nervous system innervates the gut. The enteric neurons are originally derived from the migratory vagal NC marked by *crestin* at 36hpf (48). Knockdown of *chd7* reduced the expression of *crestin* in vagal NC cells (Fig. 5E and F) suggesting that the specification of these cells is compromised. This *chd7* MO2 had similar effects on crestin expression (Supplementary Material, Fig. S5L and S5M). The differentiated enteric neurons in 6dpf zebrafish larvae can be visualized using the Tg(*NBT*:dsRed) line that expresses a red fluorescent protein in all neuronal cell bodies. Deficiency of *chd7* led to a severe reduction in the number of enteric neurons (Fig. 5G and H). CHARGE patients have not been reported to have enteric neuronal defects, although there have been reports of chronic constipation in patients (49), which is a symptom of colonic agangliogenesis as seen in Hirschprung disease (50).

At 4dpf, the olfactory microvillous neurons are marked by *sox10*:eGFP expression (51). We visualized the effect of chd7 knockdown on these cells and found that the *chd7* morphant larvae have a reduced number and structural disorganization of the olfactory microvillous neurons (Fig. 5I and J). Chd7 mutant mice also exhibit defects in the number and organization of olfactory sensory neurons (52). The lateral line hair cells are important mechanosensory neurons in the zebrafish. We used the fluorescent dye DASPEI to visualize the lateral line neuromasts

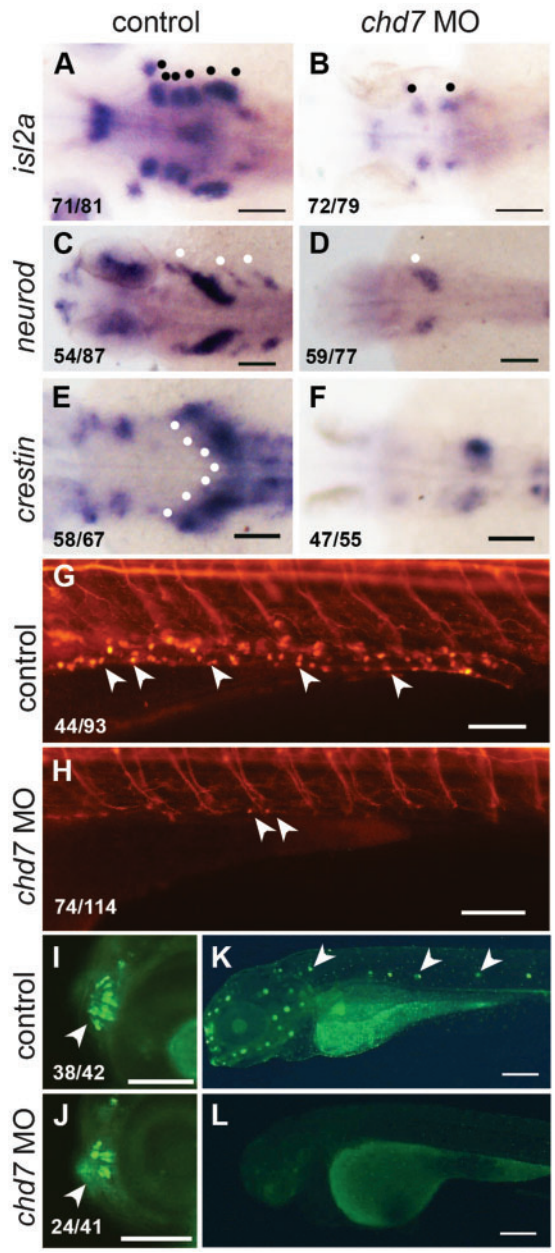

Figure 5. *chd7* knockdown causes loss of peripheral neuronal lineages. **(A, B)** RNA *in situ* hybridization of *islet 2a* at 72hpf which marks the differentiated sensory and motor cranial neurons (black dots, a) was severely reduced in *chd7* morphants. **(C, D)** The epibranchial neuronal precursors marked by *neuroD* in the head (white dots, C) was lacking in the *chd7* morphants. **(E, F)** The vagal neural crest and precursors of enteric neurons marked by *crestin* in 36hpf control embryos (white dots, E) was reduced in chd7 morphants. **(G,H)** At 6dpf, *Tg(NBT:dsRed)* marks enteric neurons on the gut tube (white arrowheads, g) was severely decreased in *chd7* morphants. **(I, J)** *Tg(sox10:eGFP)* marks well patterned and organised microvillous neurons at 4dpf (white arrowheads, i) and fewer and disorganized microvillous neurons were present in *chd7* morphants. **(K,L)** DASPIE staining highlights the neuromasts cells along lateral line in 4dpf control embryos (white arrowheads, k) and these neurons were completely absent in the *chd7* morphant embryos. All images have anterior to the left, dorsal views (A–F) and lateral views (G–L). Scale bars are 100μm (A–H, K–L) and 50μm (I–J). The numbers in the bottom left corner indicate the actual number of embryos of the total represented by the image.

and found that chd7 morphants had a significant reduction of these neurons (Fig. 5K and L). Thus, multiple sensory neuronal types are depleted in the chd7 morphant embryos.

To test whether the depletion of peripheral neurons is a result of of Sox10 deregulation, we co-injected embryos with *chd7* MO and *sox10* MO. We did not observe any rescue of the neurod, crestin or isl2a expression in the embryos co-injected with both *chd7* MO and *sox10* MO (Supplementary Material, Fig. S5A–S5I, S5P–S5R). Similarly, we analysed the co-injected embryos for olfactory and enteric neurons and did not find any significant rescue compared to *chd7* morphants (Supplementary Material, Fig. S5S and S5T). Thus, peripheral neurons derived from the neural crest are dependent on Chd7 function and this function cannot be compensated for by down-regulating *sox10* mRNA.

Loss of *chd7* Expands Glial Precursors But Inhibits Myelination of Schwann Cells in A *Sox10*-Dependent Manner

Neural crest cells give rise to a number of different kinds of glia associated with the peripheral neurons viz. satellite glia and myelinated and nonmyelinated Schwann cells (17). At 24hpf, *foxd3* is expressed in cranial glia associated with the preotic and postotic ganglia (53) and this expression was completely abolished in the *chd7* morphant embryos (Fig. 6A and B). However, at 56hpf *foxd3* expression in the trunk satellite glia associated with the dorsal root ganglia (DRG) (54) showed an increase in *chd7* morphants compared to the controls (Fig. 6C and D). We also observed an increase in the trunk glia of 4dpf *chd7* morphant larvae (Fig. 6G and H) by *foxd3* RNA *in situ* hybridization; this effect was dramatically illustrated in the Tg(*foxd3*:GFP) transgenic line (Fig. 6E and F) that marks the lateral line glia in 4dpf larvae with GFP (55).

To determine if this increase in *foxd3* positive glial cells also results in more myelinated Schwann cells we performed RNA *in situ* hybridization for myelin basic protein (mbp) mRNA. *mbp*, a specific marker of myelinated Schwann cells is prominently expressed in the lateral line and in the periocular region at 4dpf (56). Deficiency of *chd7* causes an overall decrease in the expression of *mbp*, around the eye and on the lateral line (Fig. 6K and L). This was further confirmed by quantitative RT-PCR (0.4 fold, Supplementary Material, Fig. S6H). Larvae injected with *chd7* MO2 also had a similar downregulation of mbp in the lateral line and the periocular region (Supplementary Material, Fig. S6F and S6G). The expression of *mbp* and in turn myelination is induced by the transcription factor, *krox20*. Compared to control larvae, the expression of *krox20* in the *chd7* morphant larvae was also significantly reduced (Supplementary Material, Fig. S6A and S6B).

We have thus uncovered a novel aspect of CHARGE syndrome in our zebrafish model. The severe reduction in the myelinated Schwann cells of the peripheral nervous system was accompanied by an expansion of satellite and other non-myelinated glia marked by *foxd3* in the morphant. We speculate that glial defects may contribute to many of the peripheral nervous system deficits in CHARGE patients. Micucci and colleagues have recently reported an increase in glia in the subventricular zone in the brain in Chd7 mutant mice resulting from a neuron-to-glia fate switch (57). Very recent studies by He *et al.* have shown that Chd7 and Sox10 interact to specify central nervous system glial cells in mouse (58). In our study, *chd7*

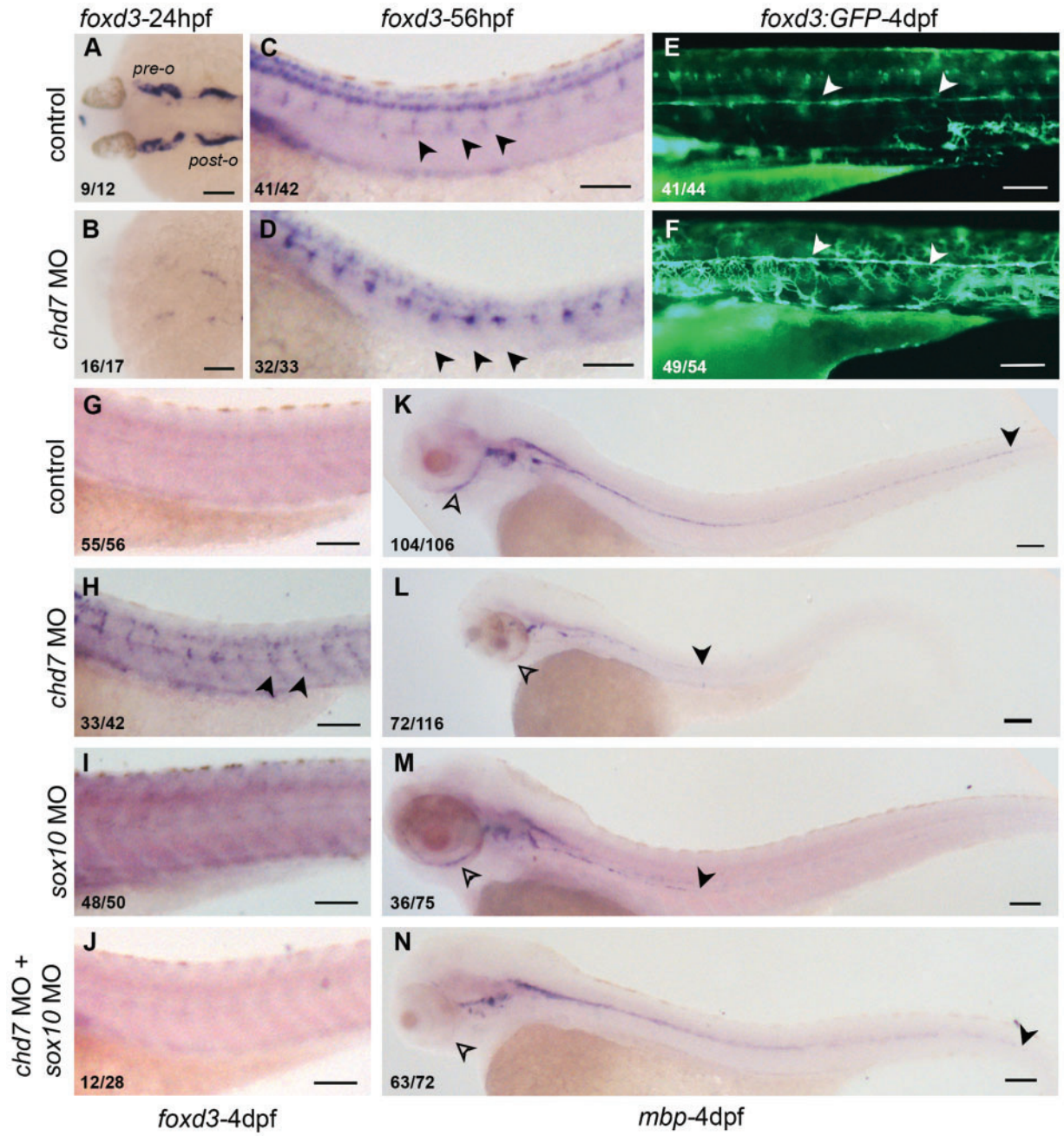

Figure 6. *chd7* knockdown leads to expanded non-myelinating glia and reduced myelinating Schwann cells in a Sox10-dependent manner. **(A, B)** Cranial glia associated with pre-otic and post-otic ganglia in 24hpf embryos was completely absent in the *chd7* morphant embryos. **(C, D)** In 56hpf embryos *foxd3* positive satellite glia associated with the dorsal root ganglia are enhanced in the *chd7* morphants. **(E, F)** *Tg(foxd3:GFP)* marks the lateral line glia in 4dpf control larvae (arrowheads, E), which shows increased fluorescence intensity with many more dentritic shaped cells present ectopically in the *chd7* morphant embryos (injected with 0.8ng of *chd7* MO) (arrowheads, F). **(G–J)** *foxd3* RNA *in situ* hybridization of 4dpf larvae does not show any signal in control, while *chd7* morphant embryos have enhanced signal. *sox10* morphants and embryos coinjected with *chd7* and *sox10* MO are not different from the control. **(K–N)** RNA *in situ* hybridization for myelin basic protein (mbp) in 4dpf embryo marks the myelinated glia. The extend of myelinating Schwann cells on the lateral line are marked by the black arrowhead and the periocular ganglia are marked by black open arrowheads. .The *chd7* morphant embryos (L) and the *sox10* morphant embryos (N) have reduced extend of lateral line glia (black arrowhead) and periocular glia (open arrowhead). Emrbyos coinjected with *chd7* MO and *sox10* MO show a recovery in the posterior extend of the lateral line Schwann cells (black arrowheads N). All images have anterior to the left, dorsal views (A–B) and lateral views (C–N). All scale bars are 100μm. The numbers in the bottom left corner indicate the actual number of embryos of the total represented by the image.

deficiency caused an expansion of glial cells in the trunk but was detrimental to myelination of these cells.

Sox10, overexpressed in 24hpf and older *chd7* morphant embryos is a known regulator of *foxd3* (59), the marker of glial precursors (55). Sox10 is also a crucial regulator of glial fate choice and myelination (60). We asked whether the glial cell phenotype in *chd7* morphants is mediated by Sox10. We knocked down *sox10* in the *chd7* morphants and observed the effects on glial fate. The expansion of *foxd3* expression in the trunk of 4dpf chd7 morphant larvae was reversed by the combined reduction of *chd7* and *sox10* (Fig. 6G and J, Supplementary Material, Fig. S6I). Further, we analysed the effect of the combined

knockdown of *chd7* and *sox10* on myelination. We found that co-injection of *chd7* MO and *sox10* MO affected a dramatic rescue of the myelinated Schwann cells; 90% of double morphant embryos showed a nearly normal lateral line expression of mbp (Fig. 6K and N and Supplementary Material, Fig. S6J) and nearly half also rescued the periocular glia. This effect was also reproduced in embryos coinjected with *chd7* MO and *sox10* MO2 (Supplementary Material, Fig. S6C–S6E).

Sox10 is a known inducer of the myelination program in the glia; however a previous study in chick embryos has shown that the overexpression of Sox10 results in inhibition of differentiation of NC derivatives, including myelinated Schwann cells (61). We therefore suggest that the overexpression of Sox10 in the *chd7* morphants is the cause of inhibition of myelination and that when this inhibition was relieved in double morphants, the *foxd3* positive glial cells differentiated into myelinated Schwann cells efficiently.

chd7 Knockdown Leads to Defects in Craniofacial Cartilage Specification and Differentiation in a Sox10-Dependent Manner

Craniofacial skeletal abnormalities are a predominant feature of CHARGE syndrome (9). Our *chd7* morphant larvae also exhibited a smaller head, smaller eyes and an absence of the lower jaw at 4dpf (Fig. 7A and B). Alcian blue staining of cartilage (Supplementary Material, Fig. S7B) and *sox10*:eGFP fluorescence in the chondrocyte stacks (Fig. 7F) in the 4dpf morphant larvae confirmed the severe reduction of craniofacial cartilage structures such as the Meckel's, Ceratohyal, and Ceratobranchial cartilages. Craniofacial defects have been reported in zebrafish (13) and mouse models (21). *chd7* MO2 caused similar but less severe jaw phenotypes (Supplementary Material, Fig. S7L).

The precursors of ectomesenchyme express transcription factors such as *dlx2a*, *sox9a* and *sox9b* that commit them to

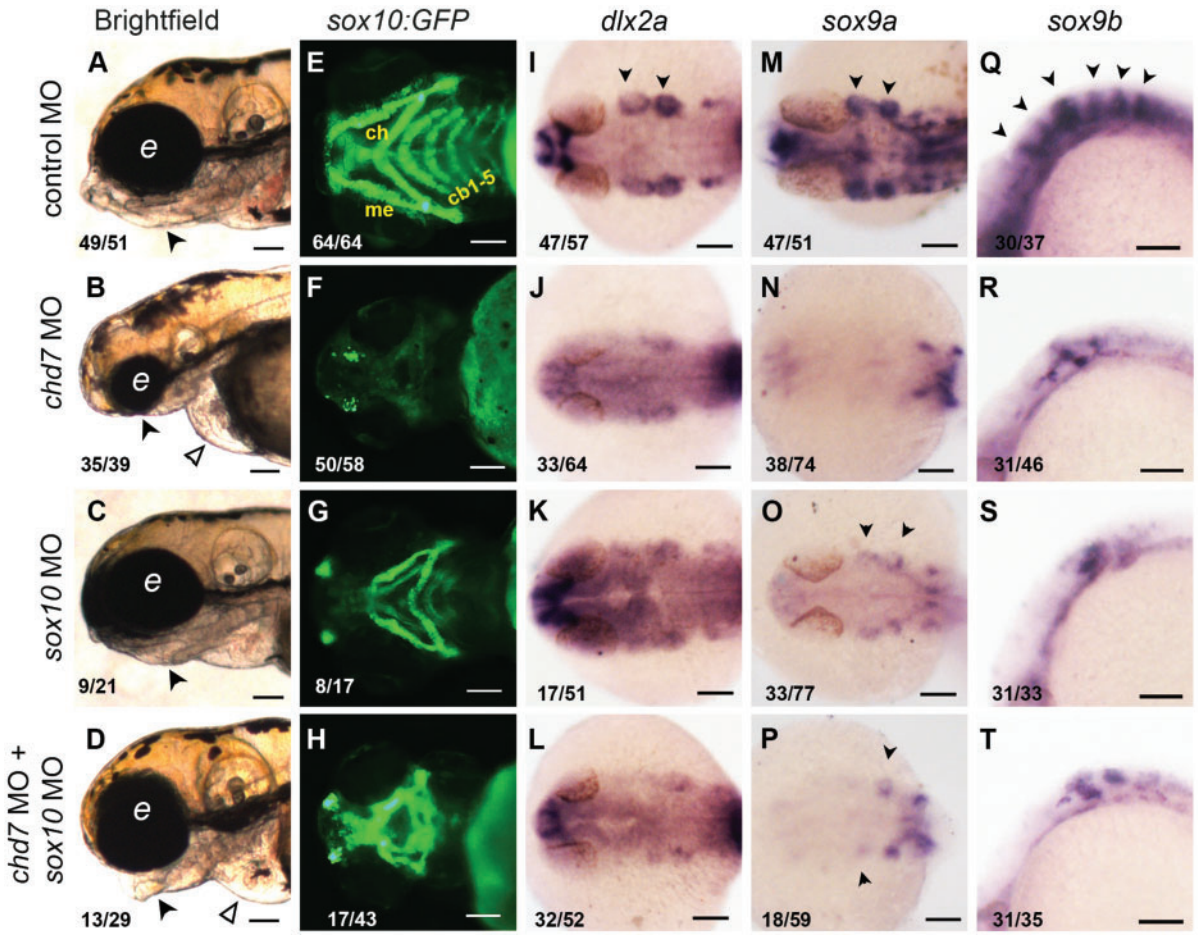

Figure 7. *chd7* knockdown leads to defects in craniofacial cartilage specification and differentiation in a Sox10-dependent manner. **(A–D)** 4dpf control larvae exhibited a well-formed lower jaw (black arrowhead, A) while *chd7* morphants had a missing lower jaw (black arrowhead, B, smaller head and pericardial edema (open arrowhead). Embryos injected with *sox10* MO had partial loss of lower jaw (black arrowhead, C). Larvae coinjected with *chd7* MO and *sox10* MO showed partial rescue of the jaw structures (black arrowhead, D). **(E–H)** *Tg(Sox10:eGFP)* marks chondrocyte stacks in the jaw of 4dpf control larvae highlighting the Meckel's (me), Ceratohyal (ch) and Ceratobranchial (cb1-5) cartilages. All major cartilage elements were absent in the *chd7* morphant larvae (F) while ceratobranchial arches were absent in Sox10 morphants (G). Larvae coinjected with *chd7* MO and *sox10* MO had recovered significant cartilage structures (H). **(I–T)** RNA *in situ* hybridization of control (I, M, Q), *chd7* MO (J, N, R), *sox10* MO (K, O, S) and *chd7* and *sox10* MO coinjected 24 hpf embryos (l, p, t). *Dlx2a* marks the migratory NC cells in the pharyngeal arches (black arrowheads, I), which was downregulated in *chd7* morphants and *sox10* morphants (K). Embryos coinjected with *chd7* and *sox10* MO did not show any recovery of *dlx2a* expression (L). (M–P) *sox9a* which marks the craniofacial cartilage precursors in the pharyngeal arches (black arrowheads, m) was completely lost in the chd7 morphants (N). *sox10* morphants had much reduced expression of *sox9a* (O). Embryos coinjected with *chd7* and *sox10* MO did not look very different from *chd7* morphants (P). (Q–T) *sox9b* marks the perichondrium bands in control embryos (black arrowheads, Q) and this expression was reduced and the bands disorganized in the *chd7* morphants (R) and *sox10* morphants (S). Embryos coinjected with *chd7* and *sox10* MO were similar to the *chd7* morphants with no rescue apparent (T). All images have anterior to the left, lateral view (A–D, Q–T) dorsal view (I–P), ventral view (E–H). All scale bars are 100μm. The numbers in the bottom left corner indicate the actual number of embryos of the total represented by the image.

cartilage fate and promote the activation of cartilage-specific genes (62). We analysed the expression of *dlx2a* in 24hpf embryos, expressed in the migratory neural crest cells that form pharyngeal arches 1-4 (62,63), and found that the *chd7* morphants showed a reduction of *dlx2a* in the arches (Fig. 7I and J). *Sox9a* and *sox9b*, two paralogs of SOX9 in zebrafish, regulate chondrogenesis in the head (62). The control embryos have robust *sox9a* and *sox9b* expression in the pharyngeal arches 1 and 2 and in the perichondrium (62) respectively. We found a severe reduction in the expression of both *sox9a* and *sox9b* genes in the *chd7* deficient embryos (Fig. 7M,N,Q,R). It has been previously shown that the CHD7 protein can bind and activate the human SOX9 enhancer (11) and our present results suggest that *sox9* might be an evolutionarily conserved target of CHD7 from zebrafish to humans.

We probed the precursor population of NC cells that give rise to the ectomesenchymal derivatives in the craniofacial region of the embryo. Migratory cranial NC cells are marked by crestin at 24hpf (64), and we observed an almost complete absence of crestin staining in the *chd7* morphant embryos (Supplementary Material, Fig. S7I and S7J). On the other hand, as described earlier, more Sox10 positive cells were present in the cranial region in the *chd7* morphants at 24hpf (Supplementary Material, Fig. S2E and S2F). This suggests that the defect in the derivatives of the neural crest in the head may be a defect of ectomesenchymal fate choice. So, could the increase in Sox10 expression contribute to a suppression of cartilage fate in the morphants? To address this, we co-injected the *chd7* MO with *sox10* MO and observed the effect on the jaw in *sox10:eGFP* larvae. Our analysis revealed that compared to 14% of chd7 morphants that have normal or partial cartilage structures, 72% of the double morphants have partial or normal cartilage (Fig. 7E and H and Supplementary Material, Fig. S7N). Using Alcian blue staining and *sox10:eGFP* fluorescence for the craniofacial cartilage we observed that both *sox10* MO1 and *sox10* MO2 caused defects and reduction in the calcification of craniofacial structures in the 4dpf larvae Supplementary Material, Fig. S7C, S7G, S7N and Fig. 7G). Upon co-injection of *chd7* MO with *sox10* MO1 or *sox10* MO2 a partial recovery of the cartilage structures were evident in the larvae (Supplementary Material, Fig. S7D, S7H, S7N). *Sox9a, sox9b* and *dlx2a* did not show significant rescue in the double morphants (Fig. 7L,P,T and Supplementary Material, Fig. S7O,S7P,S7Q). This suggests that reducing the Sox10 levels can partially rescue the craniofacial cartilage defects in the chd7 morphants, however the mechanism remains unclear. Our results support the view that the craniofacial skeletal defects in CHARGE are due to defective fate specification in the ectomesenchymal lineage and that this is caused, at least in part, by the deregulation of Sox10.

Discussion

CHARGE syndrome is a debilitating and often fatal congenital disorder. 65–70% of patients have a mutation in the chromatin remodeler CHD7 (9). Many of the tissues affected in CHARGE syndrome such as heart, auditory neurons, facial neurons and craniofacial bones (9) have their origins in the neural crest lineage. Earlier studies have also implicated a role for Chd7 in the neural crest cells (11,18,21). In this study, we aimed to systematically understand the neural crest related defects in a chd7 compromised state. Since NC is a unique vertebrate tissue type (65), we chose zebrafish the highly amenable vertebrate model organism to perform this study.

Using morpholino antisense oligonucleotides to knockdown zebrafish *chd7* we generated a model for CHARGE syndrome. Using this model we identified certain novel aspects of Chd7 function and perhaps CHARGE manifestation. We discovered defects in pigmentation, enteric neurons and myelination of Schwann cells, all previously undocumented in CHARGE patients or CHARGE models. We suggest that some of these phenotypes such as abnormalities in enteric ganglia or myelination defects may have relevance in patients and may have been overlooked just because they are not obvious during gross examination in the clinic.

The morphant zebrafish showed a selective delay in NC development with striking abnormalities in the trunk NC migration. We found that NC cells marked by *sox10*, migrate efficiently into the head NC regions but crestin positive cells were absent in the head. We interpret this as a change of fate in the cranial NC from *crestin* expressing cells to Sox10 expressing cells. We also discovered that the craniofacial cartilage, that form from the cranial NC are compromised in the *chd7* morphants. Sox10 downregulation was able to rescue these craniofacial defects indicating a role for Sox10 in the fate determination of the cranial NC.

We also documented a persistence or upregulation of Sox10 in the NC cells in the *chd7* morphant embryos. This could be a direct consequence of the delay or defect in migration of the NC in the *chd7* morphants, since Sox10 downregulation in normal NC cells is linked to their ventral migration. However, our study indicates that timely downregulation of Sox10 is an important event in the specification and differentiation of NC cells into their derivatives and that a delay in the downregulation of Sox10 can have consequences on fate choice and differentiation of NC cells. This hypothesis is borne out by the apparent rescue of craniofacial cartilage and myelination defects in *chd7* morphants by downregulation of Sox10 protein.

Thus, we conclude that Chd7 is an important player in the specification, migration, fate-choice and differentiation of NC. We also conclude that Sox10 is an important mediator of function of Chd7 in NC. We show that by external regulation of *sox10* expression, we can rescue some aspects of the neural crest derived phenotypes in the CHARGE model suggesting possible avenues of intervention in the future.

Materials and Methods

Zebrafish lines and maintenance

Zebrafish (Danio rerio) were bred, raised and maintained at 28.5 °C under standard conditions as described (66). Embryo staging was done by using both timing (hours post fertilization, hpf) and morphological features as previously described (67). For fluorescence imaging and *in situ* hybridization analysis of embryos older than 24hpf, embryos were raised in 1-phenyl-2-thiourea (PTU) (0.003% in Embryo medium), to inhibit pigment formation (68). Zebrafish handling was in strict accordance with good animal practice as defined and all experiments were performed using protocols approved by the Institutional Animal Ethics Committee (IAEC) of the CSIR-Institute of Genomics and Integrative Biology, India. The zebrafish lines used in this study are Tuebingen (TU), used as the wild-type strain, *Tg(–4.9Sox10:egfp)*^{ba2}(69), *Tg(foxd3:GFP)*(55), *Tg(mitfa:GFP)*^{w47}(70), *and Tg(NBT-dsRed)* (71).

RNA sequencing analysis

The publicly available data for RNA-seq was obtained from NCBI SRA. Developmental timepoints RNA seq data was obtained from SRP009426 (23), SRP008845 (24), ERP000016 [Zebrafish transcriptome sequencing project, PRJEB1986] PRJNA207719 (25) and SRP017135 (26), corresponds to adult tissues. The SRA data was processed into fastq format, followed by preliminary quality check (QC) by FastQC and adapter trimming using Trimmomatic (72) The data comprised of 10 developmental stages viz., 2-4 cell, 1Kcell, dome, shield, bud, 1dpf, 2dpf, 3dpf, 5dpf, 14dpf and 9 adult tissues viz. blood, brain, heart, liver, muscle, eye, spleen, ovary and testis .

Once the preliminary QC was completed the reads for respective stages and tissues were aligned on the reference genome of zebrafish (zv10) using TopHat (73). The alignment was followed by analysing the differential expression of the annotated transcripts (ens84). Differential expression of the transcripts across the 10 stages and 9 tissues of zebrafish was obtained using Cuffdiff module (73) for which Binary alignment map (BAM) files served as input obtained from TopHat. The differential expression was in terms of Fragment per Kilo base Exon per Million Reads (FPKM) scores which is used to give the relative abundance of the transcripts across the data points. The FPKM scores were further fetched for the chd transcripts and the heatmap for the same was plotted so as to visualize the expression of them across the stages and tissues of zebrafish.

Morpholino and RNA injections

The endogenous expression of genes was perturbed by injection of morpholinos. All morpholino antisense oligonucleotides (MOs) were designed and synthesized by Gene-Tools, USA. For all experiments, the minimum effective concentration was used as determined by titration experiments. Two different *chd7* splice blocking MOs have been used in this study. The first *chd7* splice blocking MO (MO1) was designed against the exon8-intron8 boundary of *chd7* transcript (ENSDART00000135230) (Supplementary Material, Fig. S1). For confirmation, other previously reported chd7 splice blocking MOs (termed here as, MO2) was also used (13).

To determine the specificity of the phenotypes observed full length human *CHD7* RNA was co-injected with *chd7* MO. pCDNA plasmid containing full length human *CHD7* was linearized with AvrII. The linear fragment was gel-eluted and transcribed using T7-ultra mRNA synthesis kit (Ambion-Thermo Fisher). The full length mRNA was purified using oligodT based mRNA purification kit (Invitrogen), run on an agarose gel for confirmation, quantitated and frozen in small aliquotes. As truncated or partially degraded *CHD7* mRNA can function as dominant negative, thawed aliquotes of mRNA were used only once. Each embryo was injected with 1.5ng of human *CHD7* RNA and 1.2ng of *chd7* MO.

sox10 knockdown was performed using a previously reported translation blocking morpholino (42) and a splice blocking morpholino designed across exon2 and intron2 hereafter termed as *sox10* MO2. Concentrations of the various MOs used in injections are: 2.4ng for both *chd7* MO1 and MO2 and *sox10* MO1, and 12ng for *sox10* MO2. A standard control scrambled sequence MO obtained from Gene Tools® was used in all experiments as a control. All injections were done at one-cell staged embryos. Morpholinos were suspended in nuclease free water to form a stock solution of 1mM. Working solutions were made by dissolving in nuclease free water and used within 2–3 days . The list of MO sequences is given in Supplementary Material, Table S1)

Polymerase chain reaction

Total RNA was extracted by homogenizing 15–20 pooled embryos using Trizol reagent (Invitrogen). RNA was further treated with DNase (Ambion) to remove genomic DNA contamination. Wildtype (zebrafish and human) as well as aberrant chd7 transcripts were detected using RT-PCRs. Quantitative real time PCR was carried out as described (74) on the Roche LightCycler® Real-Time PCR System. For quantification, the relative standard curve method was used (as described by the manufacturer) to generate raw values representing arbitrary units of RNA transcript. Each experiment was performed on three independent occasions in biological triplicates of pooled embryos (in every experiment). Statistical analyses on normalized data were performed using $2^{-\Delta\Delta CT}$ algorithm (known as the delta-delta-Ct or ddCt algorithm) (74,75). All genes were normalized against *RPL13α* unless mentioned otherwise. All primers used in this study are listed in Supplementary Materials Tables S4, S5 and S6.

Imaging

Embryos (staged between 1 and 6dpf) were monitored and scored for phenotypes using Zeiss (Stemi 2000C®) bright field microscope (with AxiocamICc1). For visualizing iridophores, reflected light with the black background was used. For fluorescent imaging, Zeiss AxioScope A1 microscope (with Axiocam HRc®) was used. Images were captured using Zeiss proprietary software and processed and analysed in Adobe® Photoshop®.

Wholemount RNA *in situ* hybridization and immunohistochemistry

RNA *in situ* hybridization was performed as described (76). Probes of the following genes were used: *sox2, snai1b, Sox10, foxd3, tfap2a, sox9a, dlx2a, crestin, mitfa* and *dct* (77); *sox9b* (62), *neurod* (78), *isl2* (79), *tyr* (80), *mbp* (56) and *krox20* (81).

To generate a probe for chd7 a 525bp fragment of the chd7 gene was PCR amplified from 24hpf zebrafish cDNA (Primer sequences in the Supplementary Material, Table S2). The fragment was cloned into pCR4-TOPO® vector and was used as template for *in vitro* transcription of antisense *chd7* RNA probe. Images were processed as mentioned earlier.

Immunostaining for Sox10 was performed broadly as described (82). The embryos were fixed in 4% paraformaldehyde and were dehydrated through a graded methanol series. Further, the embryos were incubated with anti-Sox10 Ab (1:100 dilution) (GTX128374, Gene Tex®) for 24hrs and goat anti-rabbit IgG secondary antibody conjugated with Alexa fluor 488 was used (1:500 dilution) (A-11008, Thermo Fisher Scientific®).

Fluorescence Assorted Cell Sorting (FACS) Analysis

At 24hpf, live embryos were dechorionated with Pronase and de-yolked in ice-cold Ringers solution using a micropipette tip. Single cell suspension of the de-yolked embryos was prepared using TrypLe™ Express (Thermo Fisher Scientific®). The cells were collected, washed with ice-cold Ringers solution and passed through a 70μm filter to avoid cell clumping. The cells were then collected and re-suspended in DPBS with 2.5% FBS.

The cells were analysed for GFP + ve cells in BD FACS Aria III®. Uninjected *sox10:eGFP* positive embryos were used as controls. FACS data were analysed using BD FACSDiva™ software.

Alcian blue staining

Alcian blue stain was used to visualize the structure of the craniofacial skeleton of zebrafish as described previously (83).

DASPEI staining

DASPEI (2-(4-(dimethylamino)styryl)-N-ethylpyridinium iodide) stains hair cells within lateral line neuromasts of live zebrafish embryos. The staining procedure was carried out as described (84).

Melanin content

Melanin content was determined as described previously in (85). Embryo lysates were prepared for both control embryos and *chd7* morphants, at 2dpf and 4dpf. The sample pellet was dissolved in 1 N NaOH at 100 °C for 50 min. Optical density was measured at 490 nm, and the sample results were compared with a standard curve of known concentrations (0–300 μg/ml) of melanin (Sigma). The experiment was performed on three or more independent occasions; with sample size, i.e. number of embryos ≥50, and same for both control and *chd7* MO, each time. For relative comparison, melanin content per embryo (μg) was plotted against sample.

Supplementary Material

Supplementary Material is available at *HMG* online.

Acknowledgements

We thank Alessandro Mongera, Prateek Mahalwar and Soundhar Ramsay for generous help and for reagents. We thank Archana Vats and D. Ayyappa Raja for help with FACS analysis and Manish Kumar for confocal microscopy. We thank Vivek Natarajan and Mageshi Kamaraj for comments and discussion.

Conflict of Interest Statement. None declared.

Funding

This work was supported by Council of Scientific and Industrial Research (CSIR), New Delhi [BSC0118 to C. S., research fellowships to Z.A. and S. K. and BSC0403 for the microscopy facility], National Institutes of Health-National Institute of Dental and Craniofacial Research [R01DE024584 to R. B.] and CHARGE Syndrome Foundation Grant [R.B.].

References

1. Marfella, C.G.A. and Imbalzano, A.N. (2007) The Chd family of chromatin remodelers. *Mutat Res-Fund Mol M*, **618**, 30–40.
2. Schnetz, M.P., Bartels, C.F., Shastri, K., Balasubramanian, D., Zentner, G.E., Balaji, R., Zhang, X., Song, L., Wang, Z., Laframboise, T., *et al.* (2009) Genomic distribution of CHD7 on chromatin tracks H3K4 methylation patterns. *Genome Research*, **19**, 590–601.
3. Engelen, E., Akinci, U., Bryne, J.C., Hou, J., Gontan, C., Moen, M., Szumska, D., Kockx, C., van IJcken, W., Dekkers, D.H.W., *et al.* (2011) Sox2 cooperates with Chd7 to regulate genes that are mutated in human syndromes. *Nat Genet*, **43**, 607. U153.
4. Bouazoune, K. and Kingston, R.E. (2012) Chromatin remodeling by the CHD7 protein is impaired by mutations that cause human developmental disorders. *Proc. Natl Acad. Sci. U S A*, **109**, 19238–19243.
5. Schnetz, M.P., Handoko, L., Akhtar-Zaidi, B., Bartels, C.F., Pereira, C.F., Fisher, A.G., Adams, D.J., Flicek, P., Crawford, G.E., Laframboise, T., *et al.* (2010) CHD7 targets active gene enhancer elements to modulate ES cell-specific gene expression. *Plos Genet*, **6**, e1001023.
6. Zentner, G.E., Hurd, E.A., Schnetz, M.P., Handoko, L., Wang, C.P., Wang, Z.H., Wei, C.L., Tesar, P.J., Hatzoglou, M., Martin, D.M., *et al.* (2010) CHD7 functions in the nucleolus as a positive regulator of ribosomal RNA biogenesis. *Hum. Mol. Genet.*, **19**, 3491–3501.
7. Pagon, R.A., Graham, J.M., Jr., Zonana, J. and Yong, S.L. (1981) Coloboma, congenital heart disease, and choanal atresia with multiple anomalies: CHARGE association. *J. Pediatr.*, **99**, 223–227.
8. Vissers, L.E.L.M., van Ravenswaaij, C.M.A., Admiraal, R., Hurst, J.A., de Vries, B.B.A., Janssen, I.M., van der Vliet, W.A., Huys, E.H.L.P.G., de Jong, P.J., Hamel, B.C.J., *et al.* (2004) Mutations in a new member of the chromodomain gene family cause CHARGE syndrome. *Nat. Genet.*, **36**, 955–957.
9. Zentner, G.E., Layman, W.S., Martin, D.M. and Scacheri, P.C. (2010) Molecular and phenotypic aspects of CHD7 mutation in CHARGE syndrome. *Am. J.Med. Genet. Part A*, **152A**, 674–686.
10. Legendre, M., Gonzales, M., Goudefroye, G., Bilan, F., Parisot, P., Perez, M.J., Bonniere, M., Bessieres, B., Martinovic, J., Delezoide, A.L., *et al.* (2012) Antenatal spectrum of CHARGE syndrome in 40 fetuses with CHD7 mutations. *J. Med. Genet.*, **49**, 698–707.
11. Bajpai, R., Chen, D.A., Rada-Iglesias, A., Zhang, J., Xiong, Y., Helms, J., Chang, C.P., Zhao, Y., Swigut, T. and Wysocka, J. (2010) CHD7 cooperates with PBAF to control multipotent neural crest formation. *Nature*, **463**, 958–962.
12. Patten, S.A., Jacobs-McDaniels, N.L., Zaouter, C., Drapeau, P., Albertson, R.C. and Moldovan, F. (2012) Role of Chd7 in Zebrafish: A Model for CHARGE Syndrome. *Plos One*, **7**.
13. Balow, S.A., Pierce, L.X., Zentner, G.E., Conrad, P.A., Davis, S., Sabaawy, H.E., McDermott, B.M. and Scacheri, P.C. (2013) Knockdown of fbxl10/kdm2bb rescues chd7 morphant phenotype in a zebrafish model of CHARGE syndrome. *Dev. Biol.*, **382**, 57–69.
14. Bosman, E.A., Penn, A.C., Ambrose, J.C., Kettleborough, R., Stemple, D.L. and Steel, K.P. (2005) Multiple mutations in mouse Chd7 provide models for CHARGE syndrome. *Hum. Mol. Genet.*, **14**, 3463–3476.
15. Hurd, E.A., Capers, P.L., Blauwkamp, M.N., Adams, M.E., Raphael, Y., Poucher, H.K. and Martin, D.M. (2007) Loss of Chd7 function in gene-trapped reporter mice is embryonic lethal and associated with severe defects in multiple developing tissues. *Mamm Genome*, **18**, 94–104.
16. Melicharek, D.J., Ramirez, L.C., Singh, S., Thompson, R. and Marenda, D.R. (2010) Kismet/CHD7 regulates axon morphology, memory and locomotion in a Drosophila model of CHARGE syndrome. *Hum. Mol. Genet.*, **19**, 4253–4264.
17. Trainor, P. (2013) *Neural Crest Cells: Evolution, Development and Disease*. Academic Press.
18. Fujita, K., Ogawa, R., Kawawaki, S. and Ito, K. (2014) Roles of chromatin remodelers in maintenance mechanisms

of multipotency of mouse trunk neural crest cells in the formation of neural crest-derived stem cells. *Mech. Dev.*, **133**, 126–145.
19. Mandalos, N., Rhinn, M., Granchi, Z., Karampelas, I., Mitsiadis, T., Economides, A., Dollé, P.a and Remboutsika, E. (2014) Sox2 acts as a rheostat of epithelial to mesenchymal transition during neural crest development. *Front Physiol.*, **5**, 345.
20. Schulz, Y., Wehner, P., Opitz, L., Salinas-Riester, G., Bongers, E.M.H.F., van Ravenswaaij-Arts, C.M.A., Wincent, J., Schoumans, J., Kohlhase, J., Borchers, A., *et al.* (2014) CHD7, the gene mutated in CHARGE syndrome, regulates genes involved in neural crest cell guidance. *Hum. Genet.*, **133**, 997–1009.
21. Sperry, E.D., Hurd, E.A., Durham, M.A., Reamer, E.N., Stein, A.B. and Martin, D.M. (2014) The Chromatin Remodeling Protein CHD7, Mutated in CHARGE Syndrome, is Necessary for Proper Craniofacial and Tracheal Development. *Dev. Dynam.*, **243**, 1055–1066.
22. Hall, J.A. and Georgel, P.T. (2007) CHD proteins: a diverse family with strong ties. *Biochem. Cell Biol.*, **85**, 463–476.
23. Pauli, A., Valen, E., Lin, M.F., Garber, M., Vastenhouw, N.L., Levin, J.Z., Fan, L., Sandelin, A., Rinn, J.L., Regev, A., *et al.* (2012) Systematic identification of long noncoding RNAs expressed during zebrafish embryogenesis. *Genome Res.*, **22**, 577–591.
24. Ulitsky, I., Shkumatava, A., Jan, C.H., Sive, H. and Bartel, D.P. (2011) Conserved function of lincRNAs in vertebrate embryonic development despite rapid sequence evolution. *Cell*, **147**, 1537–1550.
25. Kaushik, K., Leonard, V.E., Kv, S., Lalwani, M.K., Jalali, S., Patowary, A., Joshi, A., Scaria, V. and Sivasubbu, S. (2013) Dynamic expression of long non-coding RNAs (lncRNAs) in adult zebrafish. *Plos One*, **8**, e83616.
26. Kelkar, D.S., Provost, E., Chaerkady, R., Muthusamy, B., Manda, S.S., Subbannayya, T., Selvan, L.D.N., Wang, C.H., Datta, K.K. and Woo, S. (2014) Annotation of the zebrafish genome through an integrated transcriptomic and proteomic analysis. *Mol. Cell. Proteomics*, **13**, 3184–3198.
27. O'Boyle, S., Bree, R.T., McLoughlin, S., Grealy, M. and Byrnes, L. (2007) Identification of zygotic genes expressed at the mid-blastula transition in zebrafish. *Biochem. Biophys. Res. Commun.*, **358**, 462–468.
28. Jacobs-McDaniels, N.L. and Albertson, R.C. (2011) Chd7 plays a critical role in controlling left-right symmetry during zebrafish somitogenesis. *Dev Dyn.*, **240**, 2272–2280.
29. Kim, K.H. and Roberts, C.W. (2013) CHD7 in charge of neurogenesis. *Cell Stem Cell*, **13**, 1–2.
30. Feng, W., Khan, M.A., Bellvis, P., Zhu, Z., Bernhardt, O., Herold-Mende, C. and Liu, H.K. (2013) The chromatin remodeler CHD7 regulates adult neurogenesis via activation of SoxC transcription factors. *Cell Stem Cell*, **13**, 62–72.
31. Haldipur, P. and Millen, K.J. (2013) Deficits in early neural tube identity found in CHARGE syndrome. *Elife*, **2**, e01873.
32. Lee, H.C., Huang, H.Y., Lin, C.Y., Chen, Y.H. and Tsai, H.J. (2006) Foxd3 mediates zebrafish myf5 expression during early somitogenesis. *Dev. Biol.*, **290**, 359–372.
33. Honjo, Y., Kniss, J. and Eisen, J.S. (2008) Neuregulin-mediated ErbB3 signaling is required for formation of zebrafish dorsal root ganglion neurons. *Development*, **135**, 2615–2625.
34. Drerup, C.M., Wiora, H.M., Topczewski, J. and Morris, J.A. (2009) Disc1 regulates foxd3 and sox10 expression, affecting neural crest migration and differentiation. *Development*, **136**, 2623–2632.
35. Silver, D.L., Hou, L. and Pavan, W.J. (2006), In Saint-Jeannet, Jean-Pierre (eds) *Neural Crest Induction and Differentiation*. Springer, US, pp. 155–169.
36. Curran, K., Lister, J.A., Kunkel, G.R., Prendergast, A., Parichy, D.M. and Raible, D.W. (2010) Interplay between Foxd3 and Mitf regulates cell fate plasticity in the zebrafish neural crest. *Dev. Biol.*, **344**, 107–118.
37. Tryon, R.C. and Johnson, S.L. (2012) Clonal and lineage analysis of melanocyte stem cells and their progeny in the zebrafish. *Methods Mol. Biol*, **916**, 181–195.
38. Mort, R.L., Jackson, I.J. and Patton, E.E. (2015) The melanocyte lineage in development and disease. *Development*, **142**, 620–632.
39. Quigley, I.K. and Parichy, D.M. (2002) Pigment pattern formation in zebrafish: a model for developmental genetics and the evolution of form. *Microsc. Res. Tech.*, **58**, 442–455.
40. Hultman, K.A. and Johnson, S.L. (2010) Differential contribution of direct-developing and stem cell-derived melanocytes to the zebrafish larval pigment pattern. *Dev. Biol.*, **337**, 425–431.
41. Elworthy, S., Lister, J.A., Carney, T.J., Raible, D.W. and Kelsh, R.N. (2003) Transcriptional regulation of mitfa accounts for the sox10 requirement in zebrafish melanophore development. *Development*, **130**, 2809–2818.
42. Dutton, K., Dutton, J., Pauliny, A. and Kelsh, R. (2001) A morpholino phenocopy of the colourless mutant. *Genesis*, **30**, 188–189.
43. Whitlock, K.E., Smith, K.M., Kim, H. and Harden, M.V. (2005) A role for foxd3 and sox10 in the differentiation of gonadotropin-releasing hormone (GnRH) cells in the zebrafish Danio rerio. *Development*, **132**, 5491–5502.
44. Laurette, P., Strub, T., Koludrovic, D., Keime, C., Le Gras, S., Seberg, H., Van Otterloo, E., Imrichova, H., Siddaway, R., Aerts, S., *et al.* (2015) Transcription factor MITF and remodeller BRG1 define chromatin organisation at regulatory elements in melanoma cells. *Elife*, **4**, doi: 10.7554/eLife.06857.
45. Hou, L. and Pavan, W.J. (2008) Transcriptional and signaling regulation in neural crest stem cell-derived melanocyte development: do all roads lead to Mitf? *Cell Res.*, **18**, 1163–1176.
46. Lol̀ pez, B.C. and Nieto-Sampedro, M. (2003) *Glial cell function*. Gulf Professional Publishing.
47. Holzschuh, J., Wada, N., Wada, C., Schaffer, A., Javidan, Y., Tallafuss, A., Bally-Cuif, L. and Schilling, T.F. (2005) Requirements for endoderm and BMP signaling in sensory neurogenesis in zebrafish. *Development*, **132**, 3731–3742.
48. Reichenbach, B., Delalande, J.M., Kolmogorova, E., Prier, A., Nguyen, T., Smith, C.M., Holzschuh, J. and Shepherd, I.T. (2008) Endoderm-derived sonic hedgehog and mesoderm Hand2 expression are required for enteric nervous system development in zebrafish. *Dev. Biol.*, **318**, 52–64.
49. Arvedson, J., Hartshorne, T., Hefner, M., Davenport, S. and Thelin, J. (2011) Feeding issues. *CHARGE Syndrome*, 113–138. in press.,
50. Southard-Smith, E.M., Kos, L. and Pavan, W.J. (1998) Sox10 mutation disrupts neural crest development in DOM Hirschsprung mouse model. *Nat. Genet.*, **18**, 60–64.
51. Saxena, A., Peng, B.N. and Bronner, M.E. (2013) Sox10-dependent neural crest origin of olfactory microvillous neurons in zebrafish. *Elife*, **2**, e00336.
52. Layman, W.S., McEwen, D.P., Beyer, L.A., Lalani, S.R., Fernbach, S.D., Oh, E., Swaroop, A., Hegg, C.C., Raphael, Y.,

Martens, J.R., *et al*. (2009) Defects in neural stem cell proliferation and olfaction in Chd7 deficient mice indicate a mechanism for hyposmia in human CHARGE syndrome. *Hum. Mol. Genet.*, **18**, 1909–1923.
53. Kelsh, R.N. and Eisen, J.S. (2000) The zebrafish colourless gene regulates development of non-ectomesenchymal neural crest derivatives. *Development*, **127**, 515–525.
54. Kelsh, R.N., Dutton, K., Medlin, J. and Eisen, J.S. (2000) Expression of zebrafish fkd6 in neural crest-derived glia. *Mech. Develop.*, **93**, 161–164.
55. Gilmour, D.T., Maischein, H.M. and Nusslein-Volhard, C. (2002) Migration and function of a glial subtype in the vertebrate peripheral nervous system. *Neuron*, **34**, 577–588.
56. Brosamle, C. and Halpern, M.E. (2002) Characterization of myelination in the developing zebrafish. *Glia*, **39**, 47–57.
57. Micucci, J.A., Layman, W.S., Hurd, E.A., Sperry, E.D., Frank, S.F., Durham, M.A., Swiderski, D.L., Skidmore, J.M., Scacheri, P.C., Raphael, Y., *et al*. (2014) CHD7 and retinoic acid signaling cooperate to regulate neural stem cell and inner ear development in mouse models of CHARGE syndrome. *Hum. Mol. Genet.*, **23**, 434–448.
58. He, D., Marie, C., Zhao, C., Kim, B., Wang, J., Deng, Y., Clavairoly, A., Frah, M., Wang, H. and He, X. (2016) Chd7 cooperates with Sox10 and regulates the onset of CNS myelination and remyelination. *Nat. Neurosci.*, **19**, 679–689.
59. Nelms, B.L. and Labosky, P.A. (2010) Transcriptional control of neural crest development. *Dev. Biol*, **1**, 1–227.
60. Britsch, S., Goerich, D.E., Riethmacher, D., Peirano, R.I., Rossner, M., Nave, K.A., Birchmeier, C. and Wegner, M. (2001) The transcription factor Sox10 is a key regulator of peripheral glial development. *Gene Dev.*, **15**, 66–78.
61. McKeown, S.J., Lee, V.M., Bronner-Fraser, M., Newgreen, D.F. and Farlie, P.G. (2005) Sox10 overexpression induces neural crest-like cells from all dorsoventral levels of the neural tube but inhibits differentiation. *Dev. Dynam.*, **233**, 430–444.
62. Yan, Y.L., Willoughby, J., Liu, D., Crump, J.G., Wilson, C., Miller, C.T., Singer, A., Kimmel, C., Westerfield, M. and Postlethwait, J.H. (2005) A pair of Sox: distinct and overlapping functions of zebrafish sox9 co-orthologs in craniofacial and pectoral fin development. *Development*, **132**, 1069–1083.
63. Akimenko, M.A., Ekker, M., Wegner, J., Lin, W. and Westerfield, M. (1994) Combinatorial Expression of 3 Zebrafish Genes Related to Distal-Less - Part of a Homeobox Gene Code for the Head. *J. Neurosci.*, **14**, 3475–3486.
64. Tu, C.T., Yang, T.C., Huang, H.Y. and Tsai, H.J. (2012) Zebrafish arl6ip1 is required for neural crest development during embryogenesis. *Plos One*, **7**, e32899.
65. Le Douarin, N.M. and Dupin, E. (2012) The neural crest in vertebrate evolution. *Curr. Opin. Genet. Dev.*, **22**, 381–389.
66. Westerfield, M. (2000) *The zebrafish book: a guide for the laboratory use of zebrafish (Danio rerio)*. 4th edn University of Oregon Press.
67. Kimmel, C.B., Ballard, W.W., Kimmel, S.R., Ullmann, B. and Schilling, T.F. (1995) Stages of embryonic development of the zebrafish. *Dev. Dynam.*, **203**, 253–310.
68. Karlsson, J., von Hofsten, J. and Olsson, P.E. (2001) Generating transparent zebrafish: a refined method to improve detection of gene expression during embryonic development. *Marine Biotechnol.*, **3**, 522–527.
69. Carney, T.J., Dutton, K.A., Greenhill, E., Delfino-Machin, M., Dufourcq, P., Blader, P. and Kelsh, R.N. (2006) A direct role for Sox10 in specification of neural crest-derived sensory neurons. *Development*, **133**, 4619–4630.
70. Curran, K., Raible, D.W. and Lister, J.A. (2009) Foxd3 controls melanophore specification in the zebrafish neural crest by regulation of Mitf. *Dev. Biol.*, **332**, 408–417.
71. Peri, F. and Nusslein-Volhard, C. (2008) Live imaging of neuronal degradation by microglia reveals a role for v0-ATPase a1 in phagosomal fusion in vivo. *Cell*, **133**, 916–927.
72. Bolger, A.M., Lohse, M. and Usadel, B. (2014) Trimmomatic: a flexible trimmer for Illumina sequence data. *Bioinformatics*, **30**, 2114–2120.
73. Trapnell, C., Roberts, A., Goff, L., Pertea, G., Kim, D., Kelley, D.R., Pimentel, H., Salzberg, S.L., Rinn, J.L. and Pachter, L. (2012) Differential gene and transcript expression analysis of RNA-seq experiments with TopHat and Cufflinks. *Nature Protocols*, **7**, 562–578.
74. Pfaffl, M.W. (2001) A new mathematical model for relative quantification in real-time RT-PCR. *Nucleic Acids Res.*, **29**, e45.
75. Livak, K.J. and Schmittgen, T.D. (2001) Analysis of relative gene expression data using real-time quantitative PCR and the 2(T)(-Delta Delta C) method. *Methods*, **25**, 402–408.
76. Aerne, B. and Ish-Horowicz, D. (2004) receptor tyrosine phosphatase psi is required for Delta/Notch signalling and cyclic gene expression in the presomitic mesoderm. *Development*, **131**, 3391–3399.
77. Stewart, R.A., Arduini, B.L., Berghmans, S., George, R.E., Kanki, J.P., Henion, P.D. and Look, A.T. (2006) Zebrafish foxd3 is selectively required for neural crest specification, migration and survival. *Dev. Biol.*, **292**, 174–188.
78. van der Velden, Y.U., Wang, L.Q., Cano, L.Q. and Haramis, A.P.G. (2013) The Polycomb Group Protein Ring1b/Rnf2 Is Specifically Required for Craniofacial Development. *Plos One*, **8**, e73997.
79. Appel, B., Korzh, V., Glasgow, E., Thor, S., Edlund, T., Dawid, I.B. and Eisen, J.S. (1995) Motoneuron fate specification revealed by patterned LIM homeobox gene expression in embryonic zebrafish. *Development*, **121**, 4117–4125.
80. Yang, C.T. and Johnson, S.L. (2006) Small molecule-induced ablation and subsequent regeneration of larval zebrafish melanocytes. *Development*, **133**, 3563–3573.
81. Lister, J.A., Cooper, C., Nguyen, K., Modrell, M., Grant, K. and Raible, D.W. (2006) Zebrafish Foxd3 is required for development of a subset of neural crest derivatives. *Dev Biol*, **290**, 92–104.
82. Solnica-Krezel, L. and Driever, W. (1994) Microtubule arrays of the zebrafish yolk cell: organization and function during epiboly. *Development*, **120**, 2443–2455.
83. Dingerkus, G. and Uhler, L.D. (1977) Enzyme clearing of alcian blue stained whole small vertebrates for demonstration of cartilage. *Stain Technol.*, **52**, 229–232.
84. Harris, J.A., Cheng, A.G., Cunningham, L.L., MacDonald, G., Raible, D.W. and Rubel, E.W. (2003) Neomycin-induced hair cell death and rapid regeneration in the lateral line of zebrafish (Danio rerio). *J. Assoc. Res. Otolaryngol.*, **4**, 219–234.
85. Choi, T.Y., Kim, J.H., Ko, D.H., Kim, C.H., Hwang, J.S., Ahn, S., Kim, S.Y., Kim, C.D., Lee, J.H. and Yoon, T.J. (2007) Zebrafish as a new model for phenotype-based screening of melanogenic regulatory compounds. *Pigm. Cell Res.*, **20**, 120–127.